RSC Advances

PAPER

View Article Online
View Journal | View Issue

Check for updates

Cite this: *RSC Adv.*, 2025, **15**, 34439

7-Methoxybenzofuran-triazole tethered *N*-phenylacetamides as a promising class of tyrosinase inhibitors: synthesis, biological evaluation and computational analyses against fungal and human tyrosinases

Aqsa Mushtaq,[a] Ameer Fawad Zahoor, *[a] Shagufta Kamal,[b] Mariusz Mojzych,[c] Muhammad Jawwad Saif [d] and Mashooq Ahmad Bhat *[e]

Aberrant melanogenesis results in excessive melanin production, which may lead to hyperpigmentation and related disorders. There has been extensive ongoing research to develop novel tyrosinase inhibitors as excessive activity of tyrosinase enzymes causes surplus production of melanin. Herein, we have evaluated the tyrosinase inhibition potency of a novel series of 7-methoxybenzofuran-joined *N*-phenylacetamides **16(a–j)** (synthesized in a 62–90% yield range) *via in vitro* and *in silico* analyses. The entire set of prepared derivatives **16(a–j)** demonstrated excellent inhibition potential, even more efficacious than the employed standards, *i.e.*, kojic and ascorbic acid (exhibiting IC_{50} values of 30.34 ± 1.00 μM and 11.5 ± 1.00 μM, respectively). Among the synthesized hybrids **16(a–j)**, *N*-(2-methoxyphenyl) acetamide linked benzofuran derivative **16h** was determined to be the most promising tyrosinase inhibitor (with IC_{50} = 0.39 ± 1.45 μM), followed by *N*-(3-nitrophenyl)acetamide linked benzofuran derivative **16f** (with IC_{50} = 0.76 ± 1.71 μM). *In vitro* assay findings were further authenticated by docking the potent compounds along with the standards against fungal tyrosinase. Furthermore, assessment of the tyrosinase inhibition potency of the promising hybrids **16h** and **16f** was carried out against human tyrosinase. The docking findings for potent hybrid **16h** were supported by performing molecular dynamics simulation studies, emphasizing its potent and stable interactions with fungal and human tyrosinases in comparison to the chosen standards, *i.e.*, kojic and ascorbic acid.

Received 16th July 2025
Accepted 27th August 2025

DOI: 10.1039/d5ra05084g

rsc.li/rsc-advances

Open Access Article. Published on 22 September 2025. Downloaded on 1/19/2026 9:13:00 PM.
This article is licensed under a Creative Commons Attribution-NonCommercial 3.0 Unported Licence.

Introduction

Tyrosinase is a copper-containing monooxygenase enzyme that is abundantly found in almost all types of living organisms to carry out several physiological roles, including the production of melanin.[1–3] Melanocyte-induced formation of melanin (natural pigment) is a major contributing factor towards the human skin and hair colour.[4–8] The skin color of human beings varies depending upon the melanin type and its quantity.[9] Tyrosinase is directly involved in the synthesis of melanin pigments, which are composed of an assortment of several biopolymers.[10,11] Melanin also shields and guards the skin from hazardous solar radiations and skin injuries.[12,13] In insects, tyrosinase metabolism is essential for the coloring and stiffness of their cuticles.[14]

Tyrosinase enzyme-mediated formation of L-DOPA (3,4-dihydroxyphenylalanine) *via* hydroxylation of L-tyrosine and the subsequent transformation of L-DOPA into dopaquinones during unregulated circumstances lead to the excessive accumulation of melanin.[15–17] The upsurge in the dopaquinone level occurs due to the unregulated activity of brain tyrosinase within the age-associated synthesis of neuromelanin, whose profusion is reported to result in neuronal damage causing Huntington's and Parkinson's diseases.[18–24] Moreover, melanin's excessive production due to the extravagant activity of tyrosinase has been linked with several skin disorders, including age spots, melanoma, ephelides, freckles, age spots and melisma.[25–29] Excessive pigmentation in fruits also leads to the deterioration in their quality.[30–32] Thus, the regulated production of melanin by employing tyrosinase inhibitors is the key necessity of cosmetics and food industry to overcome hyperpigmentation.

[a]*Department of Chemistry, Government College University Faisalabad, Faisalabad-38000, Pakistan. E-mail: fawad.zahoor@gcuf.edu.pk*
[b]*Department of Biochemistry, Government College University Faisalabad, Faisalabad-38000, Pakistan*
[c]*Faculty of Health Sciences Collegium Medicum, The Mazovian Academy in Płock, Pl. Dąbrowskiego 2, 09-402 Płock, Poland*
[d]*Department of Applied Chemistry, Government College University Faisalabad, Faisalabad-38000, Pakistan*
[e]*Department of Pharmaceutical Chemistry, College of Pharmacy, King Saud University, Riyadh 11451, Saudi Arabia. E-mail: mabhat@ksu.edu.sa*

© 2025 The Author(s). Published by the Royal Society of Chemistry

Open Access Article. Published on 22 September 2025. Downloaded on 1/19/2026 9:13:00 PM.
This article is licensed under a Creative Commons Attribution-NonCommercial 3.0 Unported Licence.

Owing to its role in the synthesis of melanin, tyrosinase is utilized as an effective therapeutic target to mitigate the abnormalities caused by melanogenesis.[18,33] The catalytic active region of tyrosinase involves the presence of two copper atoms enveloped by three histidine (HIS) residues.[34] Human tyrosinase (hTyr) is considered one of the significant targets to develop innovative and efficacious tyrosinase inhibitors to deal with hyperpigmentation disorders.[33,35] To date, several tyrosinase inhibitors have been developed (structures of some notable tyrosinase inhibitors have been given in Fig. 1). However, only a few of them are practically employed to overcome and mitigate the effects of hyperpigmentation, as most of the commonly utilized and available *anti*-tyrosinase agents are at the risk of induced toxicity. For example, the frequently employed well-known *anti*-tyrosinase agents are azelaic acid **1**, kojic acid **2**, hydroquinone **3** and arbutin **4**. These renowned inhibitors are copiously leveraged in cosmetics, and are determined to be significant hallmarks to cure melanogenesis and hyperpigmentation. However, these standard inhibitors have been extensively studied, disclosing their carcinogenic and toxic side effects.[36–38] These factors have prompted chemists to devise and discover novel, safe and effective tyrosinase inhibitors to treat dermatological disorders induced by the irregular activity of tyrosinase enzyme.

Heterocyclic organic molecules are of significant interest for synthetic chemists due to their broad-spectrum pharmaceutical profiles.[39–42] Benzofuran scaffolds and their derivatives have been found to illustrate a wide pharmacological spectrum,[43–50] as several benzofuran-endowed heterocyclic functionalities are known to play a significant role in medicinal chemistry.[51–55] Various naturally occurring and synthetically produced benzofuran derivatives exhibit a wide array of biological applications, thereby acting as potent *anti*-cancer,[56–59] *anti*-fungal,[60,61] *anti*-viral,[62] non-specific β-adrenoceptor antagonist,[63] *anti*-arrhythmic[64,65] and *anti*-tyrosinase agents.[66,67]

Our research group has earlier endeavored to develop tyrosinase inhibitors by employing the pharmaceutical properties of several heterocyclic hybrids, including benzofuran-oxadiazoles[66,67] and coumarin-triazole[68] hybrids. Here, in order to design and develop more efficacious tyrosinase inhibitors by taking into account the wide biological significance and medicinal potential of benzofuran based hybrids, we aimed to design a novel library of 7-methoxybenzofuran triazole joined with *N*-phenylacetamides **16(a–j)** to discover their *anti*-tyrosinase potential *via in vitro* and *in silico* approaches. The synthesized hybrids were subjected to *in vitro* screening against fungal tyrosinase to determine the most potent compounds with promising tyrosinase inhibitory activity. In light of the significance of computational studies, the interaction details of the synthesized potent hybrids with the fungal tyrosinase protein were analyzed *via* molecular docking analysis. In addition, to determine the efficacy of these developed promising inhibitors as skin-whitening agents, their molecular docking analysis with human tyrosinase protein (hTyr) was carried out. Molecular dynamic simulation analysis was also carried out to verify the stability of the most promising inhibitor **16h** against fungal and human tyrosinases.

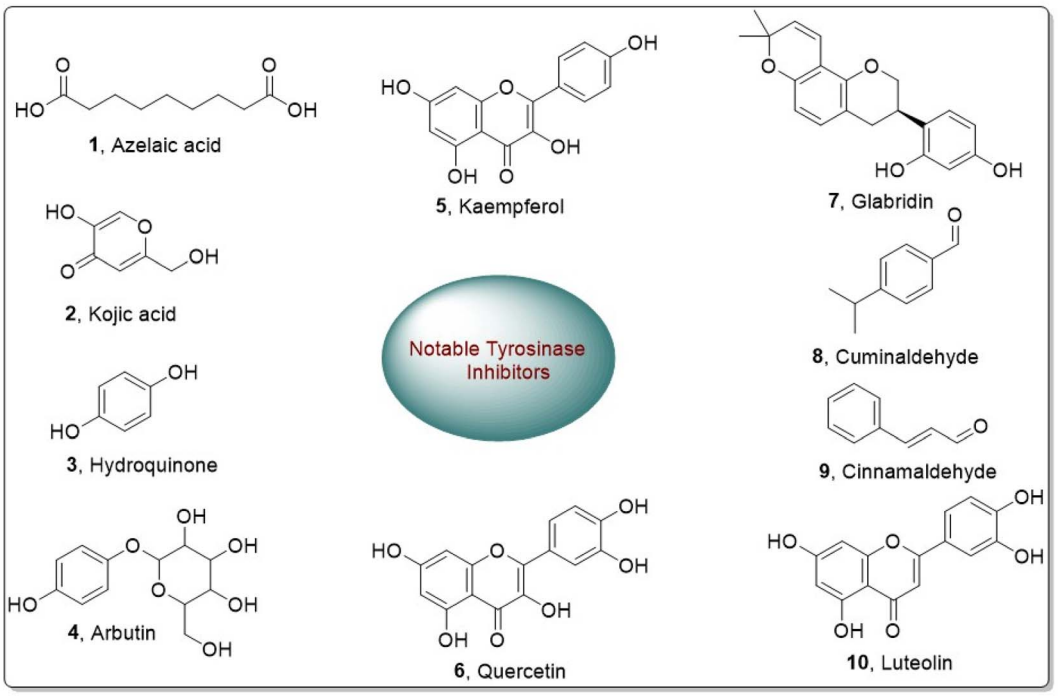

Fig. 1 Structures of a few notable tyrosinase inhibitors.

© 2025 The Author(s). Published by the Royal Society of Chemistry

Open Access Article. Published on 22 September 2025. Downloaded on 1/19/2026 9:13:00 PM.
This article is licensed under a Creative Commons Attribution-NonCommercial 3.0 Unported Licence.

Results and discussions

Chemistry

The synthetic layout for the preparation of 7-methoxybenzofuran-based triazole-acetamide derivatives has been provided in Schemes 1 and 2. Initially, the 7-methoxybenzofuran-based ester was synthesized in 69% yield by treating *o*-vanillin **11** with $ClCH_2COOEt$ (ethyl chloroacetate) **12** involving potassium carbonate (base) in DMF.[68] The synthesized ester then yielded the respective hydrazide **13** (in 98% yield) as a result of treatment with hydrazine monohydrate in methanol.[68] Afterwards, 7-methoxybenzofuran-based hydrazide **13** was reacted further to attain respective triazole **14** (in 74% yield) on exposure with phenyl isothiocyanate, followed by sodium hydroxide-induced nucleophilic cyclization in distilled water as per reported protocol[68] (Scheme 1). The resulting 7-methoxybenzofuran-based triazole **14** was made to react with a library of substituted acetanilides **15** (prepared by the nucleophilic substitution reaction of substituted anilines and bromoacetyl bromide using pyridine in DCM[66]) in the presence of potassium carbonate, using DMF as a solvent, thereby resulting in an array of 7-methoxybenzofuran-based triazole-*N*-

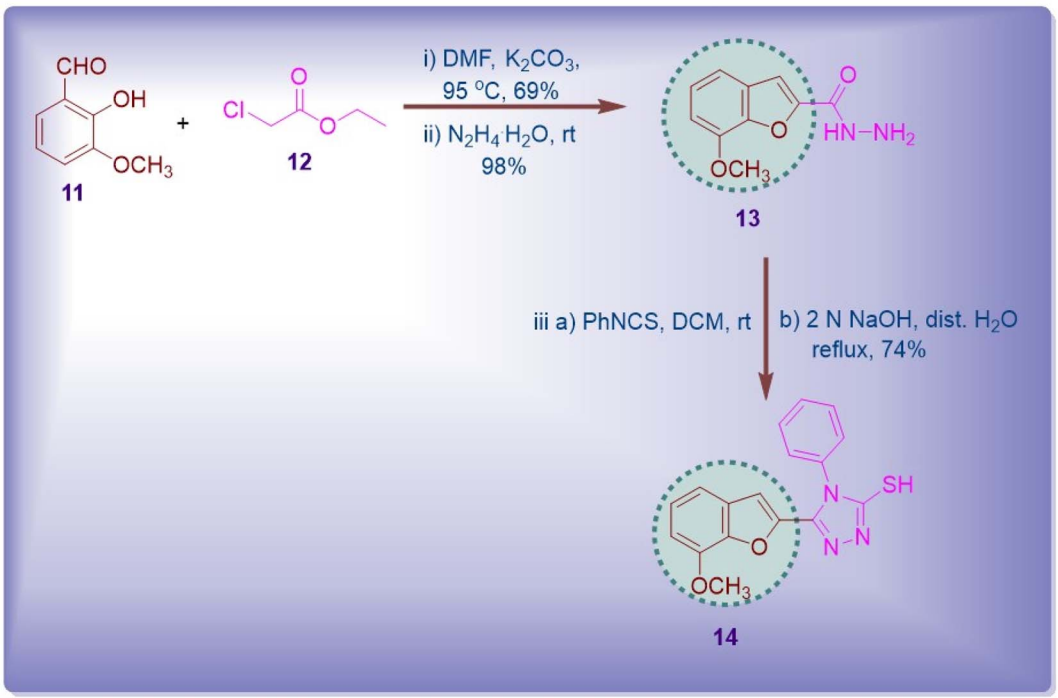

Scheme 1 Synthetic layout for the preparation of 7-methoxybenzofuran-based triazole **14**.

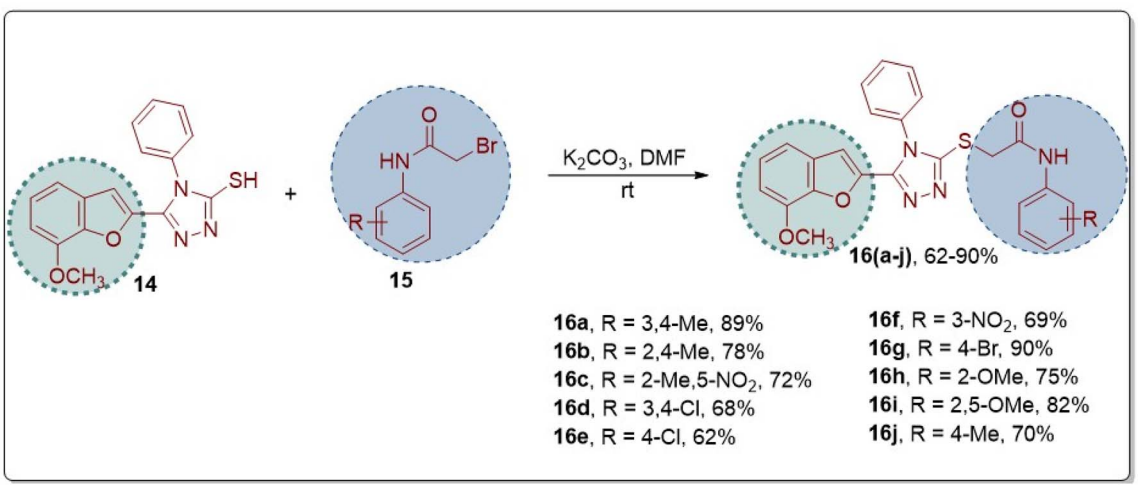

Scheme 2 Synthesis of 7-methoxybenzofuran-based triazole-acetanilide hybrids **16(a–j)**; conditions: K_2CO_3, DMF, rt, and 12–16 h.

Open Access Article. Published on 22 September 2025. Downloaded on 1/19/2026 9:13:00 PM.
This article is licensed under a Creative Commons Attribution-NonCommercial 3.0 Unported Licence.

Table 1 *In vitro* assay findings of the synthesized 7-methoxybenzofuran-triazole derivatives **16(a–j)** against fungal tyrosinase

Compound	Structure	IC_{50} (μM) ± S.E.
16a	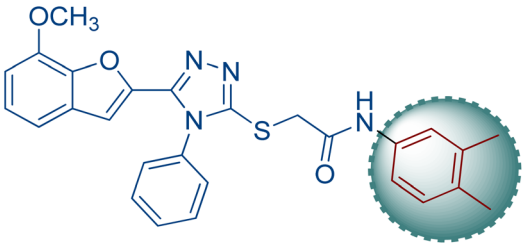	1.82 ± 5.42
16b	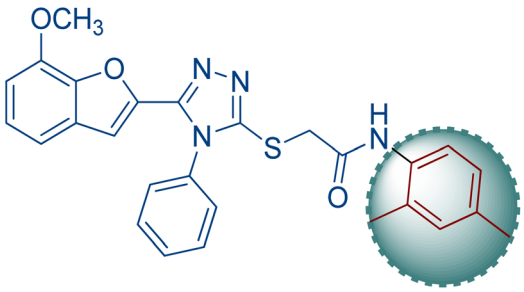	1.58 ± 5.38
16c	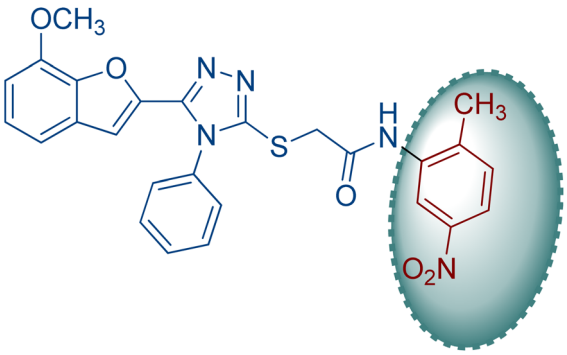	1.53 ± 2.30
16d	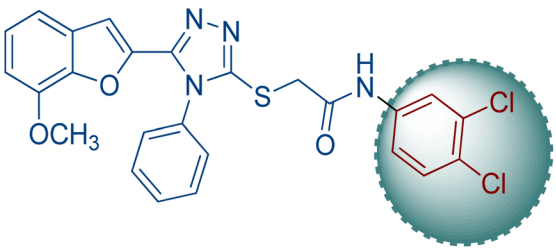	1.73 ± 3.80
16e	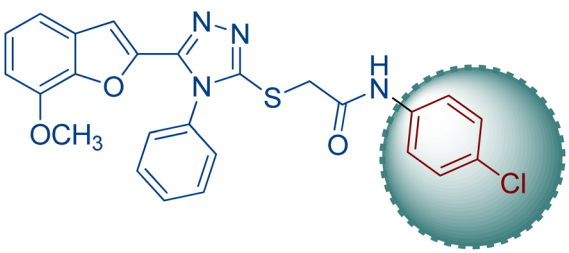	4.88 ± 1.14

© 2025 The Author(s). Published by the Royal Society of Chemistry

Table 1 (*Contd.*)

Compound	Structure	IC_{50} (μM) ± S.E.
16f	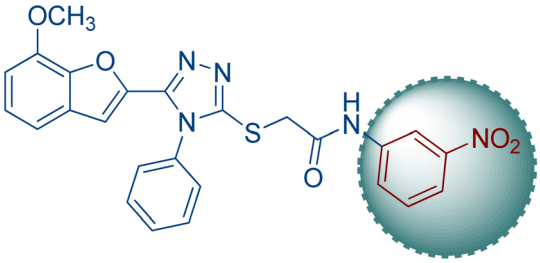	0.76 ± 1.71
16g	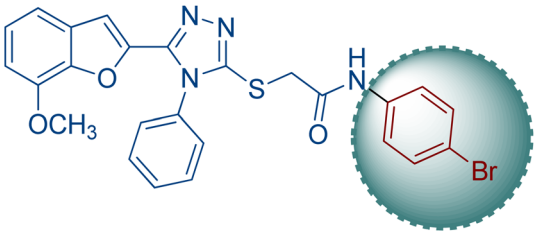	1.08 ± 4.09
16h	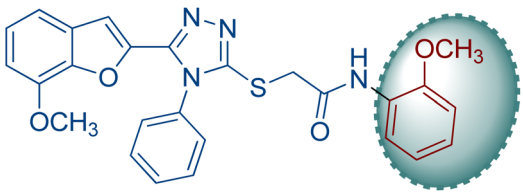	0.39 ± 1.45
16i	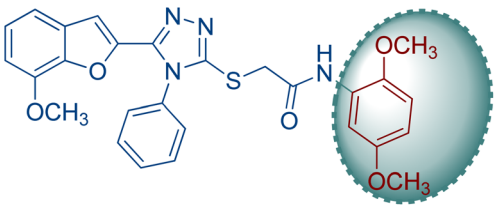	2.12 ± 5.78
16j	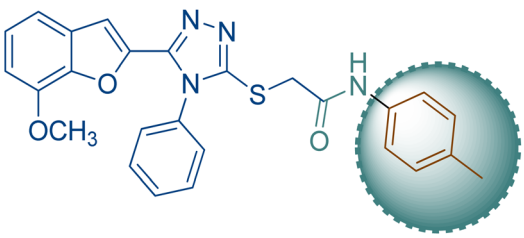	1.70 ± 3.93
Ascorbic acid	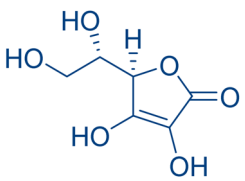	11.5 ± 1.00 (ref. 50)
Kojic acid	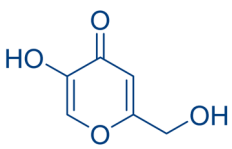	30.34 ± 1.00 (ref. 50)

Open Access Article. Published on 22 September 2025. Downloaded on 1/19/2026 9:13:00 PM.
This article is licensed under a Creative Commons Attribution-NonCommercial 3.0 Unported Licence.

Open Access Article. Published on 22 September 2025. Downloaded on 1/19/2026 9:13:00 PM.
This article is licensed under a Creative Commons Attribution-NonCommercial 3.0 Unported Licence.

phenylacetamide hybrids **16(a–j)** in moderate to excellent yield range (62–90%) (Scheme 2).

Anti-tyrosinase activity

The synthesized 7-methoxybenzofuran-triazole hybrids **16(a–j)** were analyzed for their tyrosinase inhibition potential *via in vitro* assay by employing reference inhibitors, *i.e.*, ascorbic and kojic acid. The tyrosinase assay results revealed the promising and remarkable tyrosinase inhibition activities demonstrated by all of the synthesized conjugates in comparison to that of standard inhibitors, *i.e.*, ascorbic acid and kojic acid (exhibiting IC_{50} values of 11.5 ± 1.00 μM & 30.34 ± 1.00 μM respectively) (Table 1). The half maximal inhibitory concentration of the synthesized conjugates was observed within the range of 0.39 ± 1.45 μM to 4.88 ± 1.14 μM, which indicated the efficient tyrosinase inhibition potential of the newly designed compounds. Hybrid **16h** was referred to as the most potent tyrosinase inhibitor on the basis of its lowest half-maximal inhibitory concentration (IC_{50} = 0.39 ± 1.45 μM). Meanwhile, hybrid **16f** was determined to be the second most promising inhibitor among the synthesized hybrids, thereby exhibiting the IC_{50} value of 0.76 ± 1.71 μM. In addition, hybrids **16(a–d)**, **16g** and **16j** demonstrated remarkable tyrosinase inhibition activity with IC_{50} values ranging from 1.08 ± 3.93 μM to 1.82 ± 5.42 μM. The relatively lower tyrosinase inhibition trend was observed for hybrids **16i** and **16e**, owing to their corresponding increase in half-maximal inhibitory concentration values, which were interpreted to be 2.12 ± 5.78 μM and 4.88 ± 1.14 μM, respectively.

Structure–activity relationship

The structure–activity relationship (SAR) was also deduced on the basis of varying the substitution on the phenyl ring of the phenylacetamide fragment of 7-methoxybenzofuran-joined *N*-phenyl acetamides **16(a–j)**. The SAR was inferred by considering the *in vitro* tyrosinase inhibition activity of all synthesized hybrids. The 7-methoxy benzofuran hybrid **16h** with methoxy substitution (electron donating group) at the ortho position exerted the most effective tyrosinase inhibition, as indicated by its promising IC_{50} value (0.39 ± 1.45 μM). Meanwhile, the 3-nitro (electronegative group)-substituted benzofuran hybrid **16f** also demonstrated remarkable potency by exhibiting a half-maximal minimum inhibitory concentration of 0.76 ± 1.71 μM (Fig. 2).

It was observed that di-substituted synthesized hybrids illustrated efficient tyrosinase inhibition, irrespective of their electropositive or electronegative nature, as 3,4-dimethyl and 2,4-dimethyl substituted benzofuran hybrids (**16a** & **16b**) depicted efficacious tyrosinase inhibition with IC_{50} values of 1.82 ± 5.42 μM and 1.58 ± 5.38 μM, respectively. Similarly, 7-methoxy benzofuran derivatives with 2-methyl 5-nitro substitution **16c** and 3,4-dichloro substitution **16d** also demonstrated comparable inhibition potency with **16a** & **16b**, thereby exhibiting the respective IC_{50} values of 1.53 ± 2.30 μM and 1.73 ± 3.80 μM. However, a slight increase in the IC_{50} value was observed for the 2,5-dimethoxy substituted hybrid **16i**, which was interpreted to be 2.12 ± 5.78 μM.

The trend for para substituted 7-methoxybenzofuran hybrids was determined to be quite irregular, as 4-bromosubstituted benzofuran hybrid **16g** depicted promising tyrosinase inhibition with an IC_{50} value of 1.08 ± 4.09 μM. However, the para-methyl substituted derivative **16j** exhibited tyrosinase inhibition with a relative increase in the IC_{50} value, *i.e.*, 1.70 ± 3.93 μM. Among all, the highest IC_{50} value (*i.e.*, 4.88 ± 1.14 μM) was illustrated by derivative **16e** with 4-chloro substitution on the phenyl ring.

Overall, all of the synthesized hybrids demonstrated efficacious tyrosinase inhibition with a slight dependence upon the nature and number of substituents on the phenyl ring with few

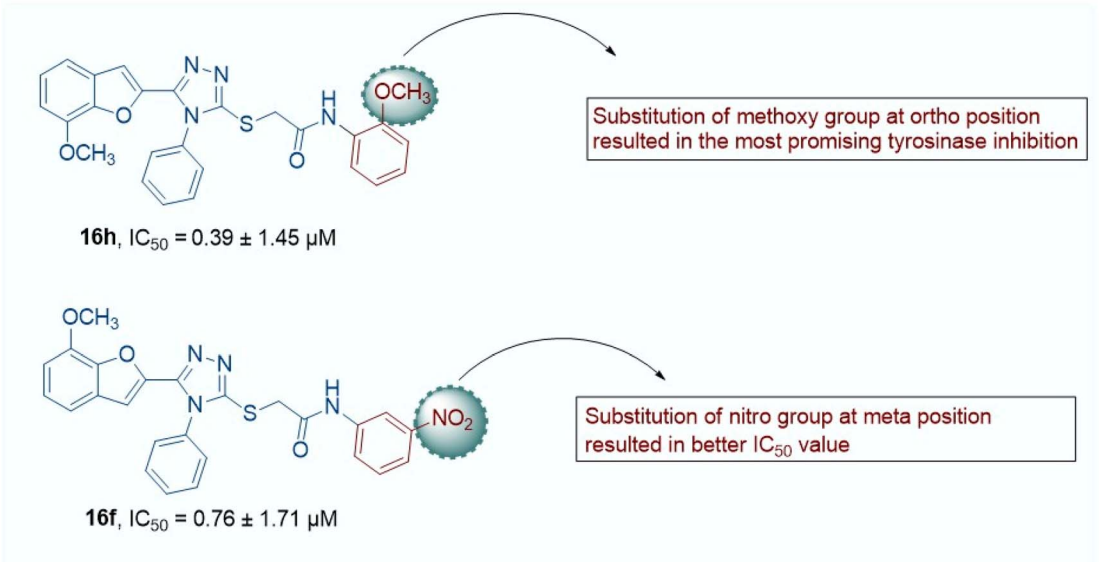

Fig. 2 Pictorial layout of the SAR of the most promising bacterial tyrosinase inhibitors **16h** and **16f**.

© 2025 The Author(s). Published by the Royal Society of Chemistry

Open Access Article. Published on 22 September 2025. Downloaded on 1/19/2026 9:13:00 PM.
This article is licensed under a Creative Commons Attribution-NonCommercial 3.0 Unported Licence.

irregularities. It was concluded that most of the mono-substituted derivatives depicted better inhibition activity than disubstituted hybrids, with the incorporation of the 2-methoxy group on the phenyl ring **16h** leading to the most promising inhibition activity.

Molecular docking analysis

Binding interactions of potent hybrids with fungal tyrosinase. The most potent compounds **16f** and **16h**, as determined by *in vitro* assay findings, were subjected to molecular docking analysis against the active site of the fungal tyrosinase protein along with standard inhibitors. The docking analysis unveiled the binding and interaction modes of these promising and standard inhibitors with the residues of the binding site. Their binding affinity scores were found to be in correlation with the *in vitro* results as hybrid **16h** displayed remarkable interactions with −9.7 kcal mol^{-1} docking score followed by hybrid **16f**, whose docking score was inferred to be −8.9 kcal mol^{-1}, indicating the significant interactions as compared to kojic (−5.5 kcal mol^{-1}) and ascorbic acids (−5.7 kcal mol^{-1}) (Table 2).

Table 2 Molecular docking scores and interactions of potent hybrids **16f** and **16h**, along with standard inhibitors

Compound	Binding score (kcal mol^{-1})	Types of interactions	Residue interacting with ligand
16h	−9.7	C–H bonding, pi–sulfur, pi-alkyl, pi-cation	ARG-195, PRO-190, MET-174
16f	−8.9	Conventional hydrogen bonding, carbon hydrogen bonding, pi-cation, pi-donor H-bonding, pi–pi T-shaped, pi-alkyl	PRO-190, ARG-195, PRO-173, TYR-194, GLY-251, MET-198
Ascorbic acid	−5.7	Conventional hydrogen bonding, carbon hydrogen bonding	ARG-195, TYR-194, PRO-173
Kojic acid	−5.5	Conventional hydrogen bonding, pi–sulfur, pi-alkyl	MET-174, PRO-190, GLN-197, ARG-195, PRO-173

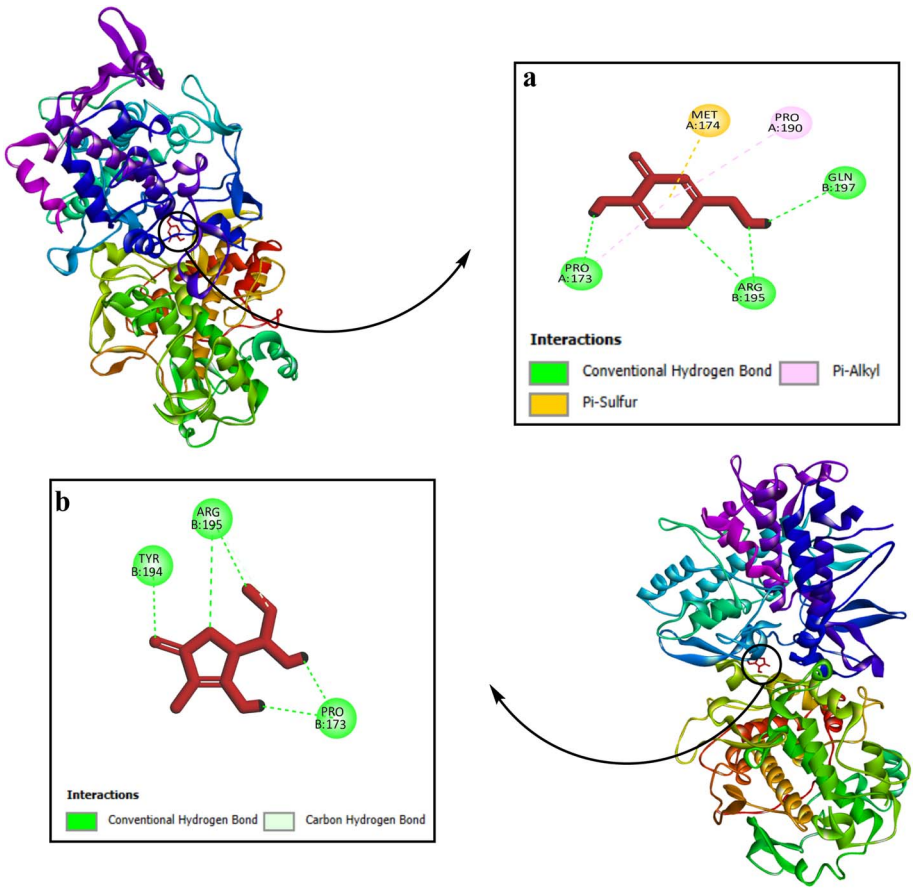

Fig. 3 Protein–ligand interactions of standard inhibitors with 6JU7: (a) kojic acid, (b) ascorbic acid.

Open Access Article. Published on 22 September 2025. Downloaded on 1/19/2026 9:13:00 PM.
This article is licensed under a Creative Commons Attribution-NonCommercial 3.0 Unported Licence.

Kojic acid (−5.5 kcal mol^{-1} docking score) displayed four conventional hydrogen bonds with ARG-195, GLN-197 and PRO-173. In addition, pi-sulfur and pi-alkyl type hydrophobic interactions were established with MET-174 and PRO-190 amino acid residues, respectively (Fig. 3). Ascorbic acid displayed a relatively better binding affinity of −5.7 kcal mol^{-1}, thereby forming six conventional hydrogen bonds with TYR-194, ARG-195 and PRO-173, along with one C–H bond with an ARG-195 amino acid residue (Fig. 3).

The most potent derivative **16h** with 2-methoxy substitution was observed to establish two conventional H-bonds with the tyrosinase's binding site, thereby illustrating a binding score of −9.7 kcal mol^{-1}. One nitrogen atom of the triazole ring and oxygen atom of the carbonyl group were determined to establish independent conventional H-bonds with ARG-195 at 2.85 Å and 2.32 Å bond distances, respectively. The triazole ring was also found to be involved in pi-cation type electrostatic interactions with ARG-195 at 3.61 Å. Besides these interactions, the phenyl ring attached to the triazole functionality formed pi-sulfur interactions with MET-174 *via* 4.95 Å bond distance. In addition, the benzofuran scaffold and phenyl ring (joined with triazole core) were observed to be engaged in several pi-alkyl type hydrophobic interactions with PRO-190 (Fig. 4).

The second promising 3-nitro substituted derivative **16f** illustrated 3 conventional hydrogen bonds along with two carbon–hydrogen bonds and one π-donor hydrogen bond. The nitrogen atom of the phenylacetamide fragment was determined to establish a conventional hydrogen bond with ARG-195 (dHB = 3.07 Å). In addition, both oxygen atoms of the $-NO_2$ group were found to display conventional hydrogen bonding interactions with ARG-195 (dHB = 2.83 Å) and TYR-194 (dHB = 2.51 Å). Meanwhile, pi-donor H-bonding interactions were observed between the phenyl ring of the phenylacetamide scaffold and TYR-194 (dHB = 3.28 Å). In addition, one oxygen atom of the nitro group and hydrogen atoms of the methoxy group formed C–H bonding with GLY-251 (3.51 Å) and MET-198 (3.42 Å), Moreover, pi-cation type hydrogen bond interactions were found between the triazole scaffold and ARG-195 (3.30 Å). In addition, the synthesized derivative **16f** illustrated several hydrophobic interactions (π–π T-shaped & π-alkyl interactions) (Fig. 5).

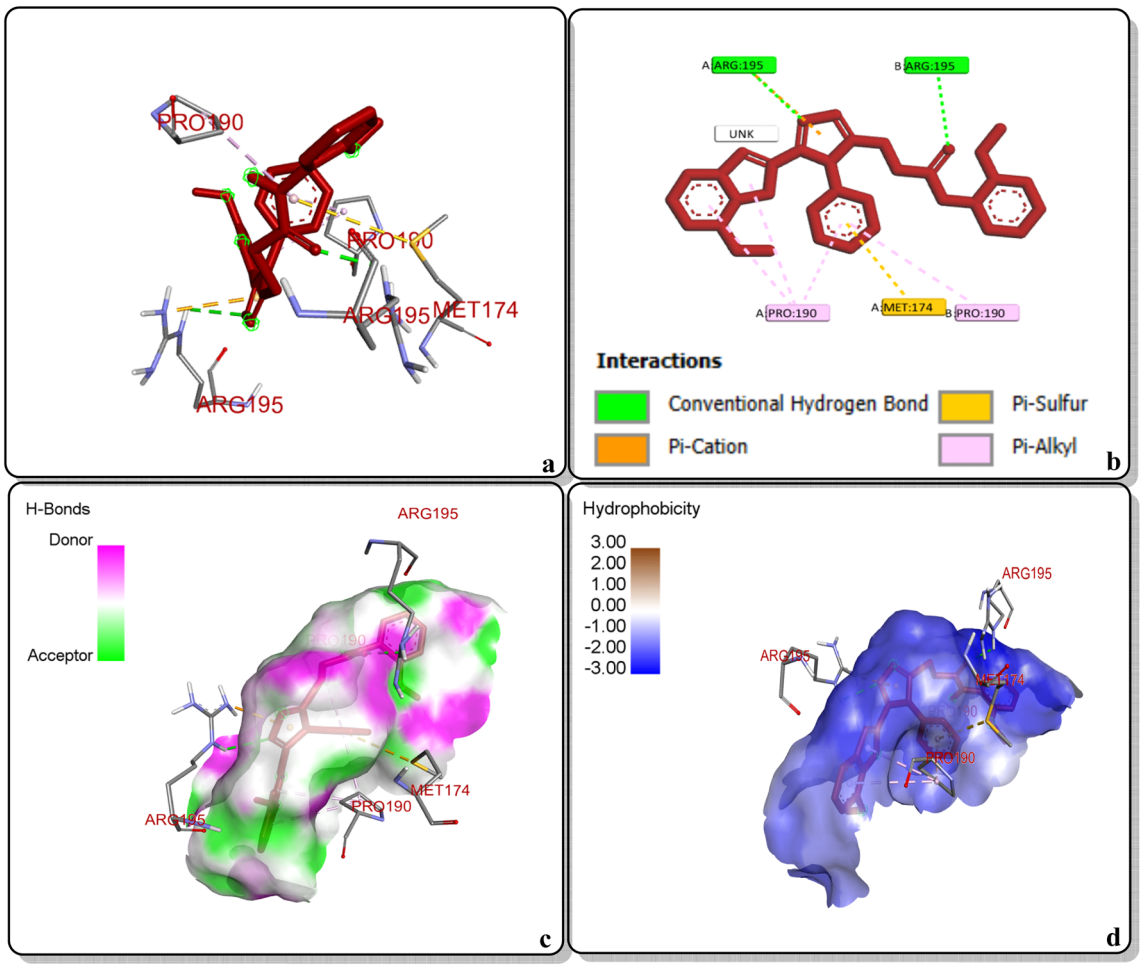

Fig. 4 Protein–ligand interactions of **16h** with 6JU7: (a) pose interaction of **16h** with the protein, (b) 2D interaction, (c) hydrogen bonding interactions, (d) Hydrophobic interactions.

© 2025 The Author(s). Published by the Royal Society of Chemistry

Open Access Article. Published on 22 September 2025. Downloaded on 1/19/2026 9:13:00 PM.
This article is licensed under a Creative Commons Attribution-NonCommercial 3.0 Unported Licence.

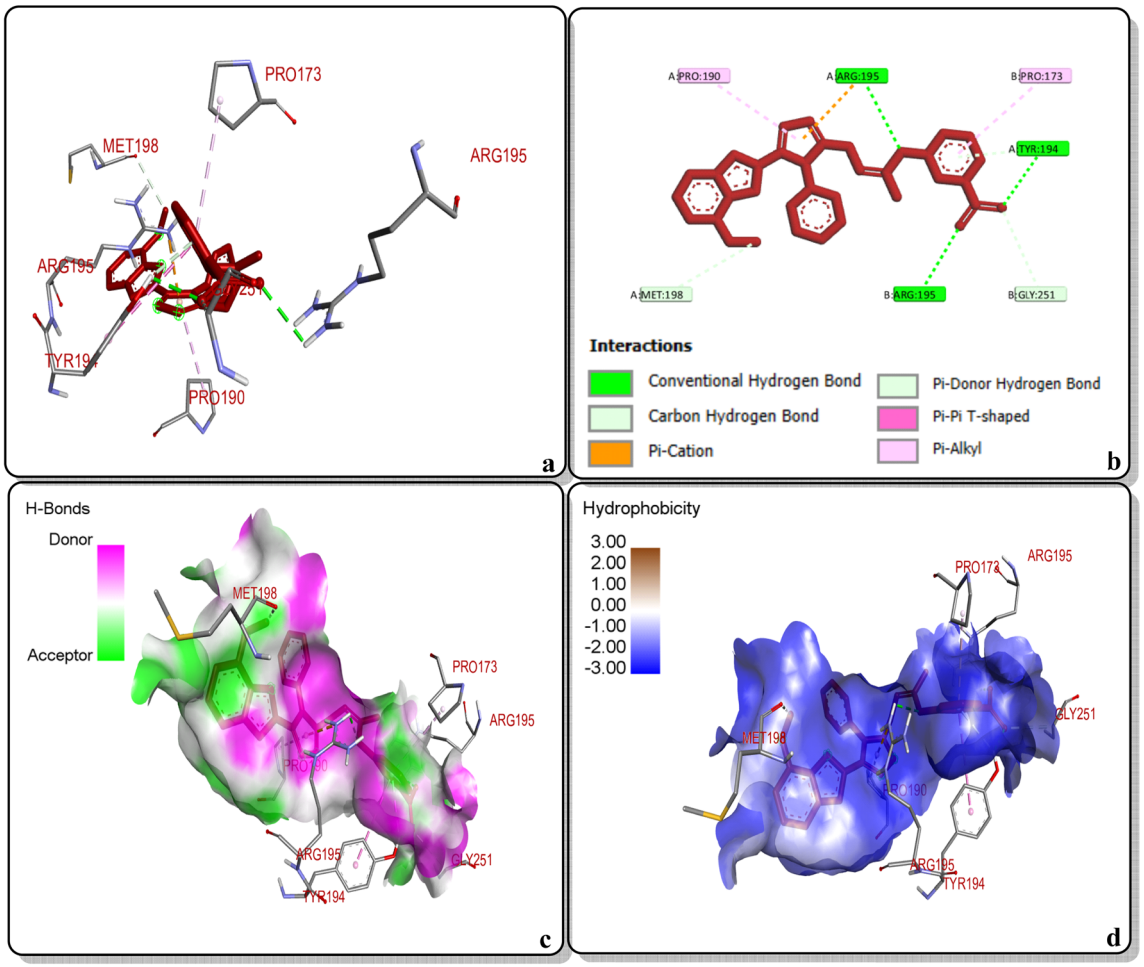

Fig. 5 Protein–ligand interactions of **16f** with 6JU7: (a) pose interaction of **16f** with the protein, (b) 2D interaction, (c) H-bonding interactions, (d) hydrophobic interactions.

Binding interactions of potent hybrids with human tyrosinase protein. Human tyrosinase protein is a metal-constituting protein involving 529 residues that are located at various sites of the cellular region, including the transmembrane, cytoplasm and signal-peptide, along with mature proteins.[69] To further determine the tyrosinase inhibition potential of **16f** and **16h** as skin-whitening agents for human skin, they were docked against hTyr (human tyrosinase) protein. As the

Table 3 Molecular docking scores and interactions of the potent hybrids **16h** and **16f**, along with standard inhibitors

Compound	Binding score (kcal mol^{-1})	Types of interactions	Residue interacting with ligand
16h	−7.7	Conventional hydrogen bonding, carbon hydrogen bonding, pi-anion, pi–pi stacked, pi–pi T-shaped, pi-alkyl	LYS-104, TYR-433, PRO-431, CYS-91, GLN-90, ASP-437, PHE-438
16f	−7.5	Conventional hydrogen bonding, pi-donor hydrogen bonding, pi-cation, pi–pi stacked, pi-sigma, pi-alkyl	PHE-347, ILE-368, VAL-377, GLN-376, LEU-279, LYS-306
Ascorbic acid	−6.7	Conventional hydrogen bonding, unfavorable acceptor–acceptor	GLN-220, PHE-107, GLN-223
Kojic acid	−6.3	Conventional hydrogen bonding, C–H bonding, pi–pi stacked, pi-alkyl	GLN-220, TRP-108, GLY-446, ARG-116, GLY-106, GLN-223

Open Access Article. Published on 22 September 2025. Downloaded on 1/19/2026 9:13:00 PM.
This article is licensed under a Creative Commons Attribution-NonCommercial 3.0 Unported Licence.

crystalline structure of human tyrosinase protein is unavailable in the protein data bank (PDB), a homology modelling operation was carried out to build the 3D homology-modeled tyrosinase protein structure (generated by using the human tyrosinase amino acid sequence from Uniprot). Both of these hybrids **16h** and **16f** interacted more efficiently with the human tyrosinase modeled protein (with −7.7 & −7.5 kcal mol^{-1} docking scores, respectively) in comparison to kojic (−6.3 kcal mol^{-1}) and ascorbic acids (−6.7 kcal mol^{-1}) (Table 3).

Ascorbic acid, being a potent standard, illustrated an efficient binding score of −6.7 kcal mol^{-1} in comparison to that of kojic acid (−6.3 kcal mol^{-1}). Ascorbic acid established two conventional H-bond interactions with PHE-107 and GLN-220 amino acids at a distance of 2.27 Å and 2.55 Å, correspondingly (Fig. 6). Meanwhile, kojic acid was found to establish five conventional hydrogen bonds (with GLN-220, ARG-116, GLN-223 and GLY-106) and one carbon hydrogen bond (with GLY-446). Moreover, π-alkyl and π–π stacked hydrophobic interactions were evident with ARG-116 and TRP-108 residues, correspondingly (Fig. 6).

The most potent compound **16h** unveiled the most promising binding score of −7.7 kcal mol^{-1}, thereby establishing two conventional hydrogen bonds and one C–H bond. The oxygen atoms of the carbonyl functionality and benzofuran ring were noted to be engaged in conventional H-bond interactions with GLN-90 (dHB = 2.42 Å) and LYS-104 (dHB = 2.37 Å), respectively. Moreover, hydrogen atoms of the methoxy group (attached to phenyl ring) were found to participate in C–H bond interactions with CYS-91 *via* 3.65 Å bond distance. The phenyl ring attached to the triazole core established pi–anion interactions with ASP-437 (4.56 Å). The PHE-347 residue developed pi–pi T-shaped interactions with the phenyl ring of phenylacetamide at 5.42 Å. Meanwhile, pi-alkyl and pi–pi stacked type hydrophobic interactions were determined between the phenyl ring (of phenylacetamide scaffold) and amino acid residues (PRO-431 & TYR-433, respectively) (Fig. 7).

The second promising hybrid **16f** also exhibited significant inhibition against the human tyrosinase modeled protein, thereby showcasing a binding affinity of −7.5 kcal mol^{-1}. The oxygen atom of the carbonyl functionality established conventional H-bonding interactions with Val-377 (dHB = 3.29 Å). Meanwhile, the phenyl ring of the phenylacetamide fragment was determined to be engaged in pi-donor H-bonding interactions with GLN-376 (dHB = 3.59 Å). In addition, pi-cation electrostatic interactions were found between the furan ring and LYS-306 (5.00 Å). Besides these interactions, the phenyl ring of the benzofuran core and the one attached to the triazole ring elicited π–π stacked and π-alkyl hydrophobic interactions with PHE-347 (5.35 Å) and VAL-377 (5.09 Å),

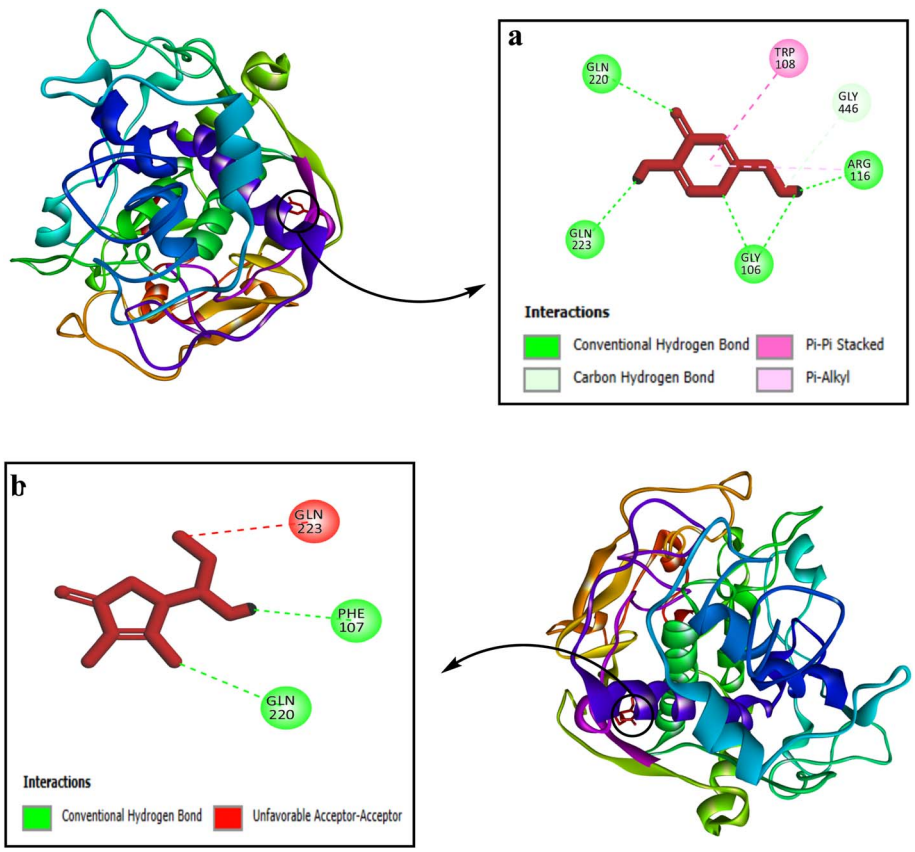

Fig. 6 Protein–ligand interactions of standard inhibitors with 5 M8T (hTyr): (a) kojic acid, (b) ascorbic acid.

© 2025 The Author(s). Published by the Royal Society of Chemistry

Open Access Article. Published on 22 September 2025. Downloaded on 1/19/2026 9:13:00 PM.
This article is licensed under a Creative Commons Attribution-NonCommercial 3.0 Unported Licence.

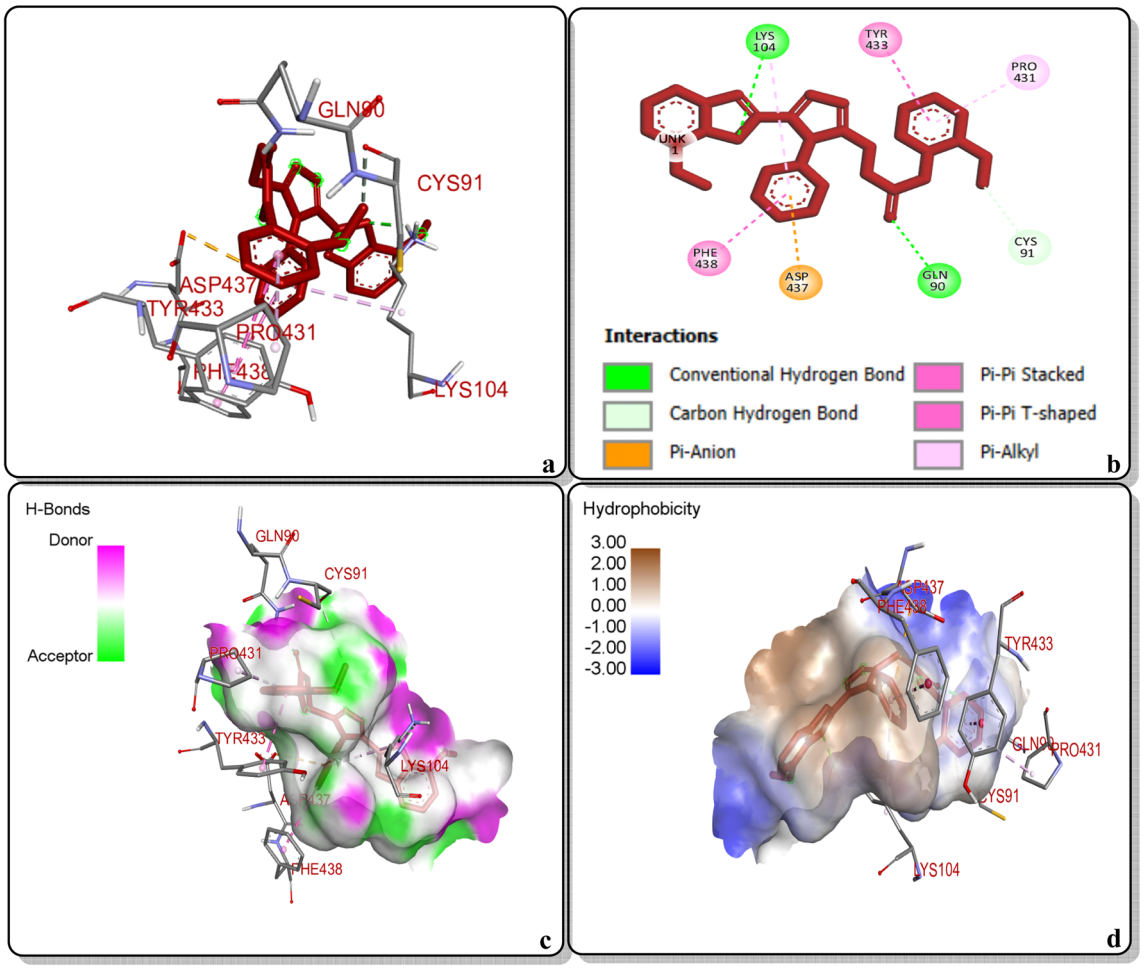

Fig. 7 Protein–ligand interactions of **16h** with 5 M8T (hTyr): (a) pose interaction of **16h** with the protein, (b) 2D interaction, (c) H-bonding interactions, (d) hydrophobic interactions.

respectively. Moreover, the phenyl ring of phenylacetamide fragment and the one attached to triazole ring formed pi-sigma type hydrophobic interactions with LEU-279 and ILE-368, respectively (Fig. 8).

Molecular dynamics simulation analysis. Molecular dynamics (MD) simulations provide dynamic confirmation of docking results, enabling a better comprehension about the stability of selected ligands and proteins. MD trajectories are used to extract several indicators such as RMSF (root mean square fluctuation), RMSD (root mean square deviation) of C–α atoms and protein–ligand contacts.

RMSD analysis of 16h with human and fungal tyrosinase. The temporal stabilities of the most potent compound **16h** and receptors (6JU7 and 5 M8T) were evaluated through 200 ns MD simulations *via* RMSD. The resulting RMSD calculations of ligands and proteins with respect to their initial states were calculated, which served as a gauge of stability for ligand–protein complex. At start, kojic acid displayed a lower RMSD with fungal tyrosinase. However, a steep incline is observed after the 180 ns period. This suggests weak binding affinity and higher conformational change. Similarly, ascorbic acid exhibited higher RMSD after the 100 ns period due to the loss of the binding affinity. The **16h**-6JU7 complex showed relatively greater stability with 6JU7 across the 200 ns simulation time Fig. 9). The root mean square deviation (RMSD) of the **16h** complex remained within a range of 2.25–2.4 Å, thereby indicating stable binding conformations. The **16h**-5M8T complex also exhibited stable interactions between the protein and ligands. The RMSD of the protein remained within 2.2–2.8 Å, while the ligand RMSD remained close to the protein RMSD throughout the simulation time. Additionally, the standards (ascorbic and kojic acids) exhibited similar fluctuations patterns as followed by the **16h** complex with human tyrosinase (Fig. 10).

RMSF analysis tyrosinase inhibitors. The MD simulation analysis *via* RMSF uncovered new patterns regarding the

Open Access Article. Published on 22 September 2025. Downloaded on 1/19/2026 9:13:00 PM.
This article is licensed under a Creative Commons Attribution-NonCommercial 3.0 Unported Licence.

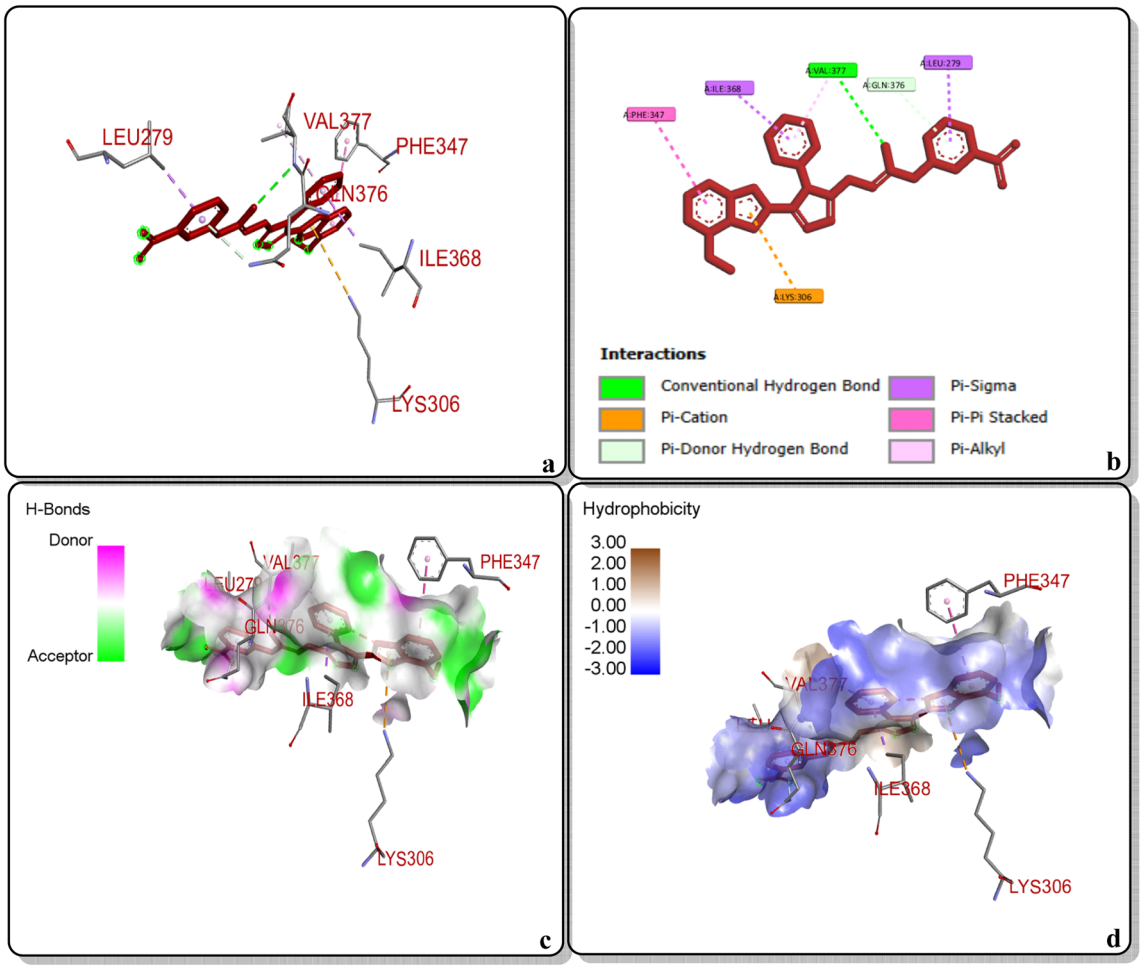

Fig. 8 Protein–ligand interactions of **16f** with 5 M8T (hTyr): (a) pose interaction of **16f** with the protein, (b) 2D interaction, (c) H-bonding interactions, (d) hydrophobic interactions.

flexibility of the potent compounds with the receptors' residues. Compound **16h** exhibited average residual flexibility with fungal tyrosinase due to flexibility in the loop region. However, no significant instability was observed. The standards kojic and ascorbic acids displayed relatively higher fluctuations specifically around 300 and 500 residues (Fig. 9). Similarly, **16h** in complex with human tyrosinase exhibited higher stability as the RMSF of most of the residues remained around 2 Å. The standard ascorbic acid showed moderate stability, but some distinct peaks were observed at residues 69–121 and 251–300 due to the local mobility of individual residues. Likewise, kojic acid displayed higher fluctuations, notably at residues 55–100 and 198–250, compared to ascorbic acid and complex **16h** (Fig. 10).

Protein–ligand contacts of 16h with human and fungal tyrosinase. To elucidate the inhibitory potential of compound **16h** against tyrosinase, insightful analysis of the potent compound's different interactions with the binding site was conducted during a 200 ns simulation time. The complex **16h** formed prominent hydrogen bonding interactions with ARG-195 (30%) *via* direct and water-mediated linkages. Similarly, the ARG-190 residue of fungal tyrosinase was determined to be engaged in the formation of hydrophobic interactions (Fig. 11). In addition, LYS-104 (44%) established water-involving H-bond interactions with the C═O group of the **16h**-5M8T complex. Likewise, the –NH group of **16h** elicited strong direct hydrogen bonding associations with the CYS-91 (59%) residue of human tyrosinase. The residue PHE-438 was also involved in the formation of hydrophobic linkages (Fig. 12). The stability of the protein–ligand complex depends upon these observed interactions during the MD simulation time.

Determination of binding free energies by using MM-PBSA analysis. The Molecular Mechanics – Poisson–Boltzmann Surface Area (MMPBSA) approach is a broadly adopted computational method for analyzing the binding affinities of

© 2025 The Author(s). Published by the Royal Society of Chemistry

Open Access Article. Published on 22 September 2025. Downloaded on 1/19/2026 9:13:00 PM.
This article is licensed under a Creative Commons Attribution-NonCommercial 3.0 Unported Licence.

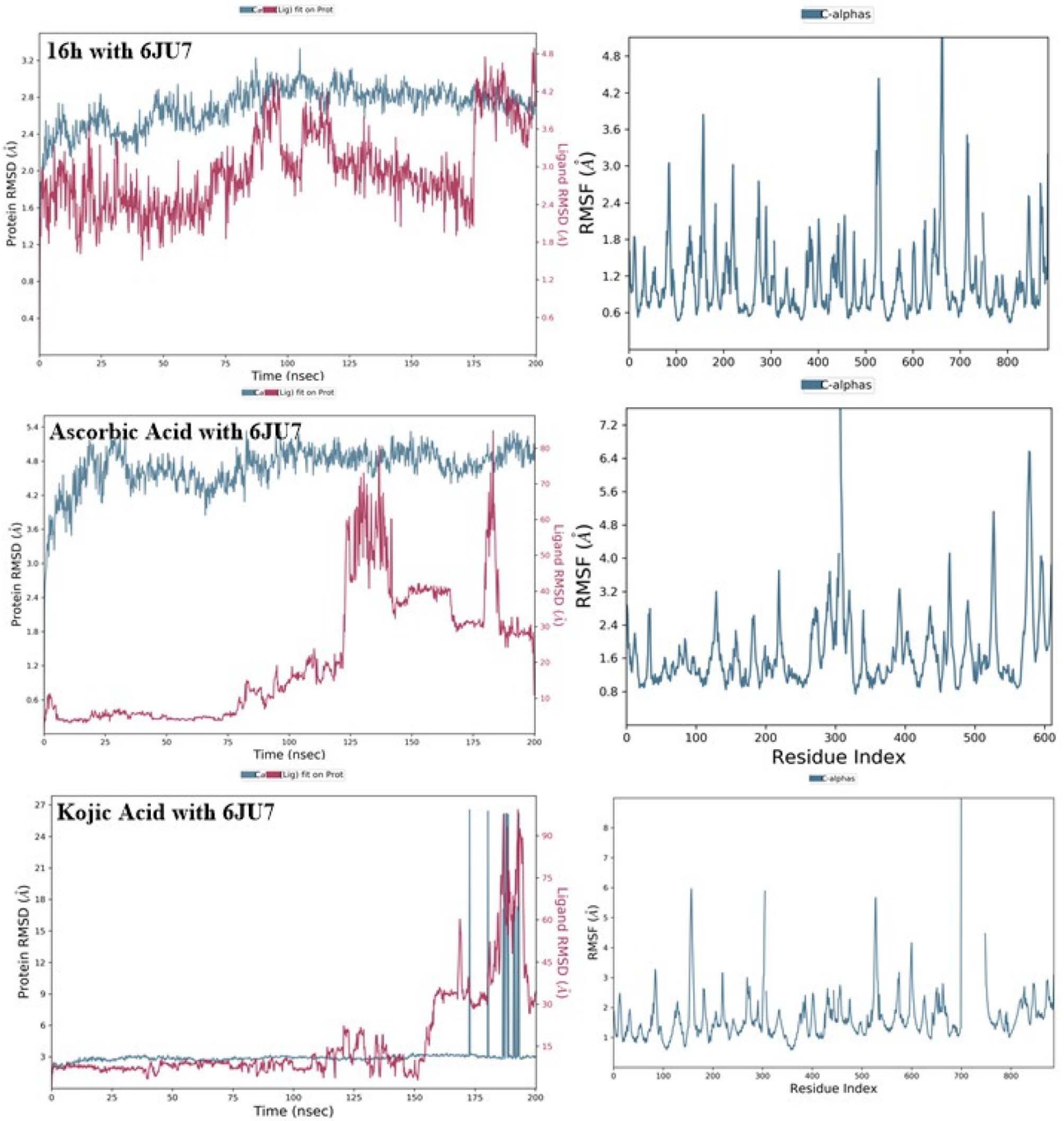

Fig. 9 RMSD and RMSF plots of **16h** and standards (kojic and ascorbic acid) with fungal tyrosinase (6JU7).

targeted ligands and proteins. In this study, MM-PBSA analysis has been performed to calculate the binding free energy of the potent compound **16h** against two different targets (6JU7 & 5M8T). The results obtained from MM-PBSA analysis are depicted in Table 4. The total binding energies of compound **16h** with receptors 6JU7 and 5M8T were found to be -88.464 kcal mol^{-1} and -59.102 kcal mol^{-1}, respectively. Table 4 shows that the van der Waal energy (-371.651 & -160.833), electrostatic energy (-34.137 & -31.863), and SASA energy (-36.59 & -18.642) play a crucial role in the binding and formation of a stable ligand–protein complex. However, the polar solvation energy (353.914 & 152.236) made a negative contribution towards the binding of the protein–ligand complex. The overall good binding energies of compound **16h**

Open Access Article. Published on 22 September 2025. Downloaded on 1/19/2026 9:13:00 PM.
This article is licensed under a Creative Commons Attribution-NonCommercial 3.0 Unported Licence.

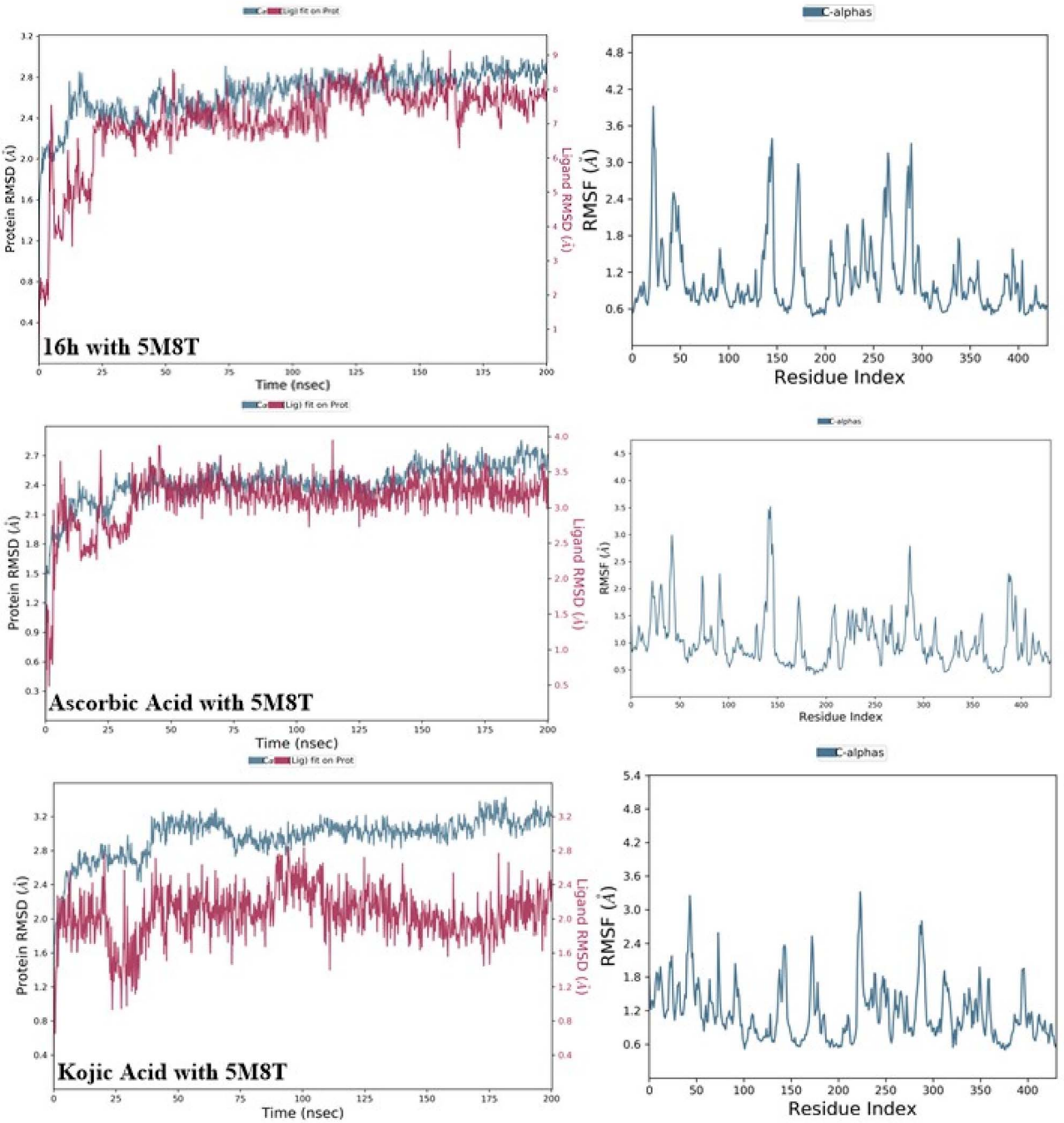

Fig. 10 RMSD and RMSF plots of **16h** and standards (kojic and ascorbic acid) with human tyrosinase (5M8T).

against both targets were found to support the experimental and computational data, thereby emphasizing its role as potential *anti*-tyrosinase agent.

ADMET analysis. ADMET analysis is one of the significant steps towards the design of efficacious drugs. Bearing in mind the efficacious *anti*-tyrosinase activities of **16f** and **16h** *via in vitro* assay and molecular docking analysis, these potent compounds were subjected to ADMET evaluation along with both standards. The ADMET profiling of these compounds revealed the physiochemical, medicinal, absorption, distribution, metabolism, excretory and toxicity parameters. Significant features of each category were studied to illustrate their

© 2025 The Author(s). Published by the Royal Society of Chemistry

Open Access Article. Published on 22 September 2025. Downloaded on 1/19/2026 9:13:00 PM.
This article is licensed under a Creative Commons Attribution-NonCommercial 3.0 Unported Licence.

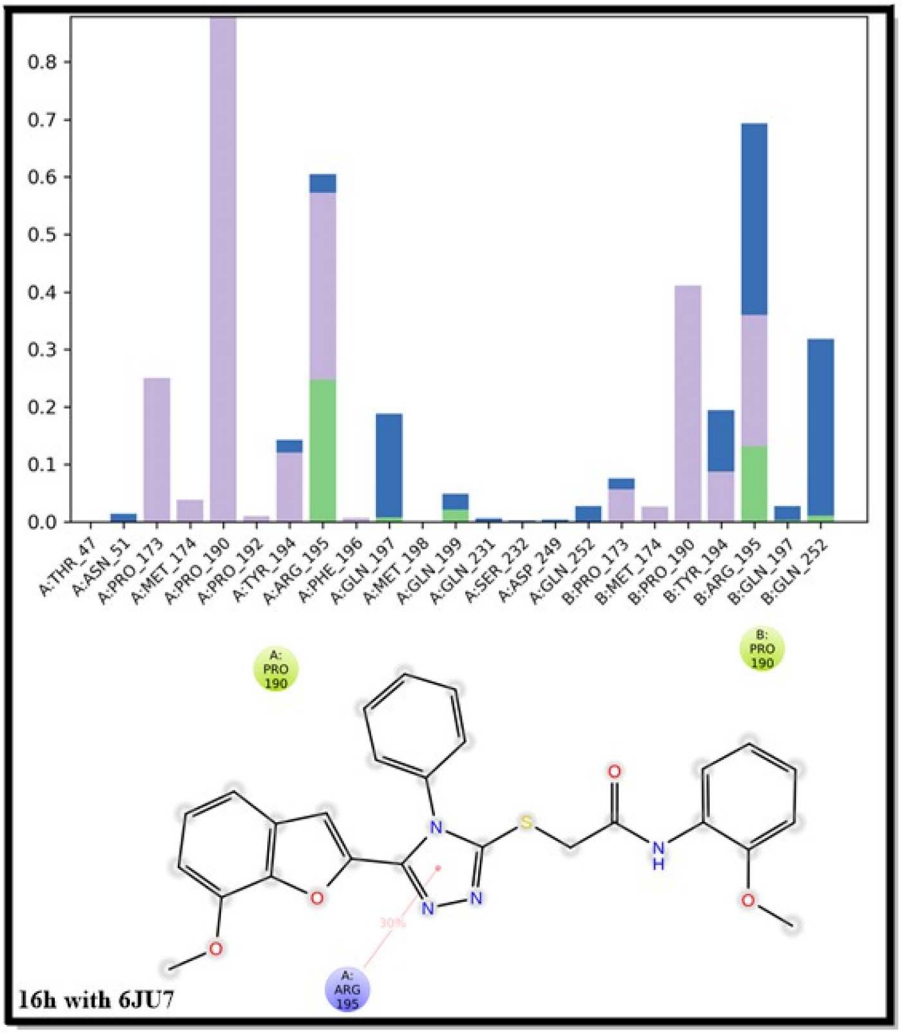

Fig. 11 Protein–ligand contacts plot of **16h** with fungal tyrosinase.

efficiency as drug-like candidates in comparison to standard inhibitors (Table 5).

The Lipinski's rule of five sets the criteria for a compound to possess certain physiochemical properties, for it to behave like a drug candidate. These properties include the molecular weight (should be ≤500 Da), log P (should be ≤5), hydrogen bond donors nHD (should be ≤5), and hydrogen bond acceptors nHA (should be ≤10). On the basis of these physiochemical features, both potent hybrids and standards were determined to follow the Lipinski's rule. The molecular weight of **16f** was determined to be more than 500. However, if a compound violates only one rule, it is still considered accepted for Lipinski's rule and can be employed as a drug-like candidate. In addition, the synthetic accessibility score was computed for each compound, and was inferred to be highly efficient for all of them.

Several absorption and distribution parameters were evaluated for the synthesized hybrids, which include human intestinal absorption (HIA), Caco-2 permeability, blood–brain barrier (BBB), Pgp inhibitor and volume distribution (VDss). The Caco-2 permeability is determined to predict the intestinal absorption of a compound. A permeability score that is higher than −5.15 is regarded as an optimal value. Hence, on this basis, the Caco-2 permeability score was evaluated to be optimal for **16f** and **16h**. However, the Caco-2 permeability score was determined to be inefficient for ascorbic acid. The HIA values were also found to be promising. The output value of BBB for the chosen compounds corresponds to their probability to invade the blood–brain barrier and affect the CNS. Similarly, the output value of Pgp-inhibitor indicates the probability of each compound to act as a Pgp-inhibitor. In addition, an output value for VD_{ss} ranging between 0.04-20 L kg^{-1} is considered as an optimal

© 2025 The Author(s). Published by the Royal Society of Chemistry

Open Access Article. Published on 22 September 2025. Downloaded on 1/19/2026 9:13:00 PM.
This article is licensed under a Creative Commons Attribution-NonCommercial 3.0 Unported Licence.

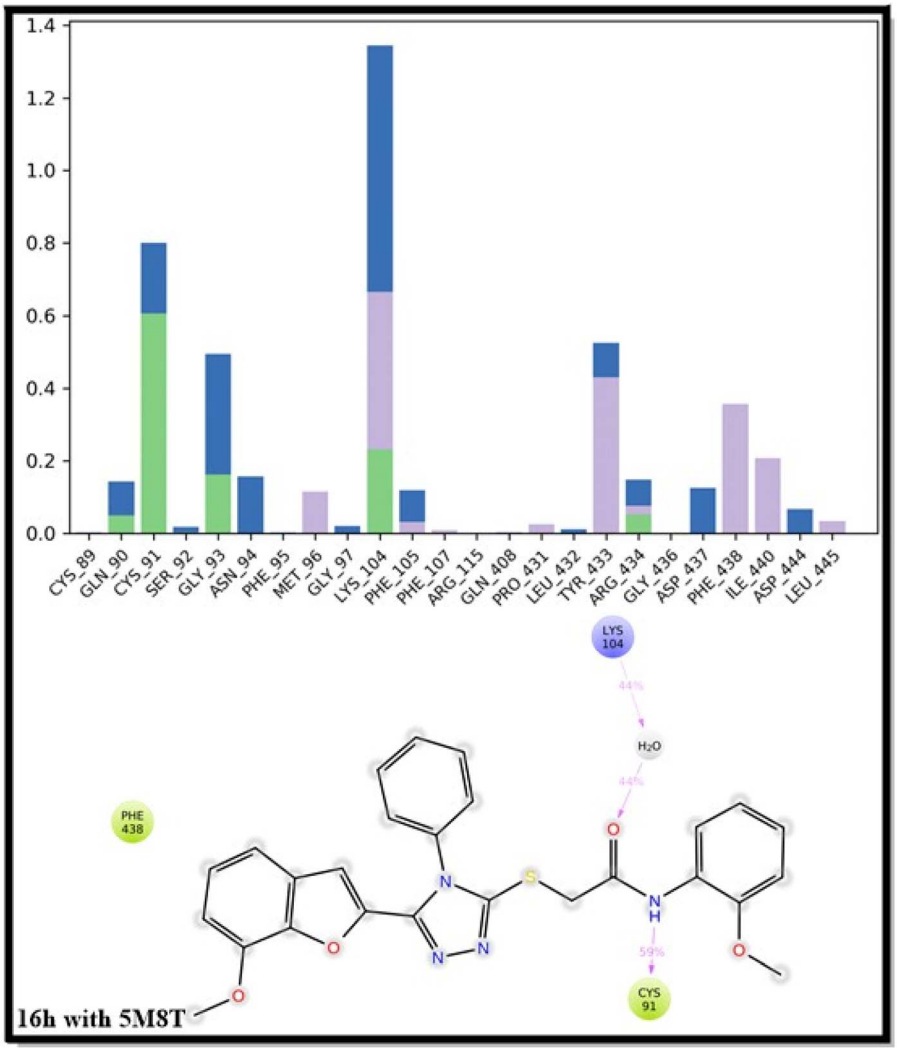

Fig. 12 Protein–ligand contacts plot of **16h** with human tyrosinase.

Table 4 Binding free energy calculations *via* MMPBSA analysis

MMPBSA (kcal mol^{-1})	**16h** (6JU7)	**16h** (5M8T)
Van der Waal energy	−371.651	−160.833
Electrostatic energy	−34.137	−31.863
Polar solvation energy	353.914	152.236
SASA energy	−36.59	−18.642
Binding energy	−88.464	−59.102

value. On this scale, only **16h** exhibited an efficient VDss score of 0.073.

The metabolism features evaluate the probabilities of selected compounds to behave as CYP2C19, CYP1A2, CYP3A4, CYP2D6, CYP2C9 and CYP2B6 inhibitors. Furthermore, CL_{plasma} values were determined to infer their clearance rate from plasma. The determined values for both potent synthesized derivatives were found to be below 5 ml/min/kg, thereby signaling low clearance and efficient absorption rate. However, CL_{plasma} values of kojic acid and ascorbic acid were inferred to be 5.51 ml/min/kg and 11.40 ml/min/kg, respectively, which signify moderate clearance. Moreover, several toxicity parameters were evaluated to determine the possible toxic effects of the prepared potent conjugates and reference inhibitors. Significantly, both **16f** and **16h** were found to be non-eye irritant, non-carcinogenic, non-respiratory toxic as well as non-rat oral acute toxic. However, hybrid **16f** exhibited an AMES-toxic output value in comparison to **16h** and the standards. Meanwhile, the output value of kojic acid indicated its carcinogenic nature. Both ascorbic and kojic acids were determined to be eye-irritants as well. These results highlight the significance of the potent compound **16h**, which has been found to be non-toxic and non-carcinogenic in all aspects.

© 2025 The Author(s). Published by the Royal Society of Chemistry

Open Access Article. Published on 22 September 2025. Downloaded on 1/19/2026 9:13:00 PM.
This article is licensed under a Creative Commons Attribution-NonCommercial 3.0 Unported Licence.

Table 5 ADMET properties of potent synthesized hybrids and standard inhibitors

ADMET properties	**16f**	**16h**	Kojic acid	Ascorbic acid
Physiochemical and medicinal properties				
Molecular weight	501.11	486.14	142.03	176.03
nHD	1.0	1.0	2.0	4.0
nHA	10.0	8.0	4.0	6.0
TPSA	125.32	91.41	70.67	107.22
nRot	9.0	9.0	1.0	2.0
LogP	3.28	3.39	−0.565	−1.707
Synthetic accessibility score	2.0	2.0	2.0	3.0
Lipinski's rule	Accepted	Accepted	Accepted	Accepted
Distribution and absorption properties				
Caco-2 permeability	−5.036	−5.007	−4.86	−6.009
BBB	0.258	0.748	0.055	0.685
HIA	0.001	0.004	0.342	0.22
Pgp-inhibitor	0.899	0.977	0.023	0.0
VDss	−0.012	0.073	−0.1	−0.449
Metabolic properties				
CYP2C19 inhibitor	0.999	1.0	0.001	0.0
CYP2B6 inhibitor	0.945	0.989	0.042	0.025
CYP1A2 inhibitor	0.927	0.677	0.068	0.083
CYP2C9 inhibitor	0.767	0.579	0.0	0.01
CYP3A4 inhibitor	0.998	1.0	0.001	0.001
CYP2D6 inhibitor	0.964	1.0	0.001	0.005
Excretion and toxicity features				
CL_{plasma}	2.70	2.63	11.40	5.51
AMES toxicity	0.92	0.61	0.64	0.45
Rat oral acute toxicity	0.63	0.49	0.46	0.084
Carcinogenicity	0.62	0.61	0.74	0.31
Respiratory toxicity	0.521	0.299	0.731	0.066
Eye irritation	0.359	0.108	0.989	0.979

Conclusion

In conclusion, our study involved the synthesis and tyrosinase inhibition screening of 7-methoxybenzofuran *N*-phenylacetamides **16(a–j)**. All of the synthesized hybrids illustrated excellent efficient tyrosinase inhibition in comparison to the standard inhibitors. The *in vitro* and *in silico* analyses showcased the remarkably excellent inhibition potential of *N*-(2-methoxyphenyl)acetamide linked benzofuran hybrid **16h** and *N*-(3-nitrophenyl)acetamide linked benzofuran hybrid **16f**, as indicated by their corresponding IC_{50} values (0.39 ± 1.45 μM & 0.76 ± 1.71 μM) and binding affinities (−9.7 kcal mol^{-1} & −8.9 kcal mol^{-1}) in comparative analysis to the utilized renowned inhibitors (*i.e.*, kojic and ascorbic acid). Furthermore, these synthesized promising inhibitors were docked against human tyrosinase protein along with standard inhibitors to evaluate their tendency as skin-whitening agents. The docking analysis unmasked the efficient interactions and binding scores of these hybrids **16h** & **16f** (−7.7 & −7.5 kcal mol^{-1}) relative to kojic and ascorbic acids (−6.3 & −6.7 kcal mol^{-1}). The docking results of the most potent hybrid **16h** were also supported by MD simulation studies. Moreover, the non-toxic and non-carcinogenic attributes of the 2-methoxy substituted benzofuran hybrid **16h** as compared to **16f** (determined by ADMET evaluation) signify its potential applicability towards the development of efficient *anti*-tyrosinase drugs by reducing the melanin production.

Experimental

Chemicals and instruments

To accomplish the synthesis of all organic molecules, the required solvents and chemicals were obtained from Sigma-Aldrich (St. Louis, MO, USA) and Macklin (China, Shanghai Pudong New Area). These chemicals and solvents were utilized within the synthetic strategy without employing any additional purification technique. The completion of the reaction was confirmed by TLC. A WRS-1B melting point apparatus was employed to determine the melting points of the synthesized compounds which were uncorrected. Furthermore, Bruker 400 MHz (for ^{1}H-MNR) and 100 MHz (for ^{13}C-NMR) NMR spectrophotometers were utilized for NMR spectroscopic analyses. Deuterated chloroform was used as the solvent and tetramethyl silane (TMS) was employed as an internal standard. The NMR spectra were interpreted *via* MestReNova software. An Agilent 6400 series (triple quadrupole QQQ) instrument was utilized to obtain the MS spectra of the synthesized compounds.

Open Access Article. Published on 22 September 2025. Downloaded on 1/19/2026 9:13:00 PM. This article is licensed under a Creative Commons Attribution-NonCommercial 3.0 Unported Licence.

General synthetic procedure

To a solution of 5-(7-methoxybenzofuran-2-yl)-4-phenyl-4*H*-1,2,4-triazole-3-thiol **14** (0.3 mmol) in DMF (5 ml), potassium carbonate (0.34 mmol) and substituted bromo acetanilides **15** (0.32 mmol) were added. The resulting mixture was left for stirring at room temperature for about 12–16 hours. Completion of the reaction was validated *via* TLC. On completion, ice cold distilled water was added to the reaction mixture while stirring at room temperature. The resultant precipitates were then filtered followed by their purification *via* column chromatography (*n*-hexane/ethyl acetate = 9 : 1). The obtained pure precipitates were further dried and weighed.

***N*-(3,4-Dimethylphenyl)-2-((5-(7-methoxybenzofuran-2-yl)-4-phenyl-4*H*-1,2,4-triazol-3-yl)thio)acetamide (16a).** Off-white solid, 89% yield, mp: 200–202 °C, ^{1}H NMR: (400 MHz, $CDCl_3$): δ 2.18 (s, 3H), 2.21 (s, 3H), 3.84 (s, 3H), 4.01 (s, 2H), 6.54 (s, 1H), 6.79 (d, J = 4 Hz, 1H), 7.03–7.13 (m, 3H), 7.36–7.62 (m, 7H), 10.08 (s, 1H). ^{13}C NMR; (100 MHz, $CDCl_3$): δ 19.1, 19.8, 36.2, 56.3, 108.3, 109.0, 113.8, 113.8, 117.3, 121.0, 124.0, 127.2, 127.2, 128.9, 129.8, 130.3, 130.3, 130.9, 132.5, 132.8, 135.8, 137.1, 142.1, 144.5, 148.0, 154.3, 166.1. MS, *m/z*: 484.9 [M^+].

***N*-(2,4-Dimethylphenyl)-2-((5-(7-methoxybenzofuran-2-yl)-4-phenyl-4*H*-1,2,4-triazol-3-yl)thio)acetamide (16b).** Off-white solid, 78% yield, mp: 81–83 °C, ^{1}H NMR: (400 MHz, $CDCl_3$): δ 2.25 (s, 3H), 2.31 (s, 3H), 3.83 (s, 3H), 4.07 (s, 2H), 6.61 (s, 1H), 6.79 (d, J = 4 Hz, 1H), 6.96–7.13 (m, 4H), 7.37 (d, J = 8Hz, 2H), 7.58–7.74 (m, 4H), 9.60 (s, 1H). ^{13}C NMR; (100 MHz, $CDCl_3$): δ 18.3, 20.9, 35.9, 56.3, 108.5, 109.1, 113.7, 122.6, 124.4, 126.9, 127.2, 127.2, 127.2, 128.9, 129.6, 130.3, 130.3, 130.3, 130.9, 131.1, 132.8, 133.3, 134.6, 142.1, 144.5, 145.5, 166.6. MS, *m/z*: 485.2 [M^+ + 1].

2-((5-(7-Methoxybenzofuran-2-yl)-4-phenyl-4*H*-1,2,4-triazol-3-yl)thio)-*N*-(2-methyl-5-nitrophenyl)acetamide (16c). Off-white solid, 72% yield, mp: 168–170 °C, ^{1}H NMR (400 MHz, $CDCl_3$); 2.52 (s, 3H), 3.83 (s, 3H), 4.11 (s, 2H), 6.57 (s, 1H), 6.79 (d, J = 8 Hz, 1H) 7.03–7.86 (m, 9H), 8.94 (s, 1H), 10.32 (s, 1H). ^{13}C NMR; (100 MHz, $CDCl_3$): δ 18.9, 36.1, 56.2, 108.7, 109.0, 113.8, 116.8, 119.2, 124.5, 127.1, 127.1, 128.8, 130.4, 130.4, 130.8, 131.1, 132.6, 136.4, 137.3, 141.8, 144.5, 145.6, 146.6, 148.2, 154.3, 166.9. MS, *m/z*: 515.9 [M^+].

***N*-(3,4-Dichlorophenyl)-2-((5-(7-methoxybenzofuran-2-yl)-4-phenyl-4*H*-1,2,4-triazol-3-yl)thio)acetamide (16d).** White solid, 68% yield, mp: 197–199 °C, ^{1}H NMR (400 MHz, $CDCl_3$): δ 3.84 (s, 3H), 4.03 (s, 2H), 6.56 (s, 1H), 6.80 (d, J = 4 Hz, 1H), 7.03–7.13 (m, 3H), 7.38–7.62 (m, 7H), 10.10 (s, 1H). ^{13}C NMR = (100 MHz, $CDCl_3$): 36.2, 56.3, 108.4, 109.1, 113.9, 117.4, 120.9, 124.4, 127.3, 127.3, 128.9, 129.8, 130.3, 130.3, 130.3, 131.0, 132.5, 132.7, 135.8, 137.0, 142.0, 144.5, 145.5, 154.4, 165.9. MS, *m/z*: 526.2 [M^+ + 2].

***N*-(4-Chlorophenyl)-2-((5-(7-methoxybenzofuran-2-yl)-4-phenyl-4*H*-1,2,4-triazol-3-yl)thio)acetamide (16e).** White solid, 62% yield, mp: 207–209 °C, ^{1}H NMR: (400 MHz, $CDCl_3$): δ 3.85 (s, 3H), 4.01 (s, 2H), 6.51 (s, 1H), 6.80 (d, J = 8 Hz, 1H), 7.03–7.13 (m, 2H), 7.38 (d, J = 8 Hz, 2H), 7.59–7.65 (m, 7H), 10.53 (s, 1H). ^{13}C NMR; (100 MHz, $CDCl_3$): δ 36.3, 56.2, 108.4, 108.9, 113.8, 121.0, 121.0, 124.4, 127.2, 127.2, 128.8, 128.8, 128.9, 129.0, 130.3, 130.3, 131.0, 132.7, 136.8, 142.0, 144.5, 145.5, 148.1, 154.3, 166.3. MS, *m/z*: 491.1 [M^+ + 1].

2-((5-(7-Methoxybenzofuran-2-yl)-4-phenyl-4*H*-1,2,4-triazol-3-yl)thio)-*N*-(3-nitrophenyl)acetamide (16f). Off-white solid, 69% yield, mp: 108–110 °C, ^{1}H NMR: (400 MHz, $CDCl_3$): δ 3.83 (s, 3H), 4.10 (s, 2H), 6.51 (s, 1H), 6.79 (d, J = 8 Hz, 1H), 7.02–7.13 (m, 2H), 7.39–7.43 (m, 3H), 7.58–7.67 (m, 3H), 7.85–7.91 (m, 2H), 8.66 (s, 1H), 10.96 (s, 1H). ^{13}C NMR; (100 MHz, $CDCl_3$): δ 36.5, 56.2, 108.5, 108.9, 113.8, 114.6, 118.7, 124.4, 125.5, 127.2, 127.2, 128.8, 129.4, 130.4, 130.1, 131.1, 132.7, 139.3, 141.8, 144.5, 145.5, 148.1, 148.5, 154.3, 166.8. m MS, *m/z*: 501.9 [M^+].

***N*-(4-Bromophenyl)-2-((5-(7-methoxybenzofuran-2-yl)-4-phenyl-4*H*-1,2,4-triazol-3-yl)thio)acetamide (16g).** White solid, 90% yield, mp: 204–206 °C, ^{1}H NMR: (400 MHz, $CDCl_3$): δ 3.84 (s, 3H), 4.02 (s, 2H), 6.54 (s, 1H), 6.80 (d, J = 4 Hz, 1H), 7.03–7.13 (m, 4H), 7.37 (d, J = 8 Hz, 2H), 7.50–7.64 (m, 5H), 10.21 (s, 1H). ^{13}C NMR; (100 MHz, $CDCl_3$): δ 36.2, 56.3, 108.4, 109.0, 113.8, 119.7, 119.7, 124.4, 127.2, 127.2, 128.9, 129.3, 129.3, 130.3, 130.3, 131.0, 132.7, 133.7, 135.6, 142.1, 144.5, 145.5, 148.0, 154.3, 166.0. MS, *m/z*: 536.3 [M^+ + 2].

2-((5-(7-Methoxybenzofuran-2-yl)-4-phenyl-4*H*-1,2,4-triazol-3-yl)thio)-*N*-(2-methoxyphenyl)acetamide (16h). White solid, 75% yield, mp: 148–150 °C, ^{1}H NMR: (400 MHz, $CDCl_3$): δ 3.83 (s, 3H), 3.92 (s, 3H), 4.12 (s, 2H), 6.70 (s, 1H), 6.78–6.93 (m, 3H), 7.00–7.13 (m, 3H), 7.37 (d, J = 8 Hz, 2H), 7.54–7.62 (m, 3H), 8.29 (d, J = 8 Hz, 1H), 9.72 (s, 1H). ^{13}C NMR; (100 MHz, $CDCl_3$): δ 36.1, 55.9, 56.4, 108.4, 109.2, 110.1, 1133.8, 120.1, 120.7, 124.1, 124.3, 127.2, 127.2, 127.2, 127.7, 129.0, 130.1, 130.1, 130.1, 130.7, 132.9, 142.3, 144.5, 145.4, 148.6, 166.1. MS, *m/z*: 486.9 [M^+].

***N*-(2,5-Dimethoxyphenyl)-2-((5-(7-methoxybenzofuran-2-yl)-4-phenyl-4*H*-1,2,4-triazol-3-yl)thio)acetamide (16i).** White solid, 82% yield, mp: 77–79 °C ^{1}H NMR (400 MHz, $CDCl_3$): δ 3.75 (s, 3H), 3.82 (s, 3H), 3.88 (s, 3H), 4.10 (s, 2H), 6.54–6.57 (m, 1H), 6.67 (s, 1H), 6.77 (t, J = 8 Hz, 2H), 7.05–7.12 (m, 2H), 7.36 (d, J = 8 Hz, 2H), 7.54–7.61 (m, 3H), 8.04 (s, 1H), 9.72 (s, 1H). ^{13}C NMR (100 MHz, $CDCl_3$) δ 36.2, 55.7, 56.4, 56.5, 106.3, 108.2, 108.9, 109.2, 111.1, 113.8, 124.3, 127.2, 127.2, 128.4, 129.1, 130.1, 130.1, 130.7, 133.0, 142.5, 142.9, 144.5, 145.4, 148.1, 153.3, 153.6, 166.2. MS, *m/z*: 516.9 [M^+].

2-((5-(7-Methoxybenzofuran-2-yl)-4-phenyl-4*H*-1,2,4-triazol-3-yl)thio)-*N*-(*p*-tolyl)acetamide (16j). Off-white solid, 70% yield, mp: 218–220 °C, ^{1}H NMR (400 MHz, $CDCl_3$): δ 2.27 (s, 3H), 3.84 (s, 3H), 4.05 (s, 2H), 6.58 (s, 1H), 6.79 (d, J = 8 Hz, 1H), 7.03–7.13 (m, 4H), 7.38 (d, J = 8 Hz, 2H), 7.51–7.64 (m, 5H), 10.21 (s, 1H). ^{13}C NMR (100 MHz, $CDCl_3$) δ 20.8, 36.3, 56.3, 108.6, 109.1, 113.8, 119.7, 119.7, 124.4, 127.3, 127.3, 128.9, 129.3, 129.3, 130.3, 130.3, 131.0, 132.7, 133.7, 135.6, 141.9, 144.5, 145.5, 147.9, 154.3, 165.9. MS, *m/z*: 470.9 [M^+].

In vitro tyrosinase assay

To ascertain the tyrosinase inhibition potency of the synthesized 7-methoxybenzofuran-joined *N*-phenylacetamides, their corresponding IC_{50} values were determined by spectroscopic methodology.[70] To carry out the tyrosinase inhibition analysis, 35 μL of the synthesized hybrid (test compound being dissolved

 © 2025 The Author(s). Published by the Royal Society of Chemistry

Open Access Article. Published on 22 September 2025. Downloaded on 1/19/2026 9:13:00 PM. This article is licensed under a Creative Commons Attribution-NonCommercial 3.0 Unported Licence.

in dimethylformamide), phosphate buffer solution (having pH = 6.8, 0.05 mM) and 765 μL of 2 mM L-tyrosine were added together and subjected to incubation for ten minutes at an optimized temperature. After 10 minutes of incubation, the isolated fungal tyrosinase enzyme (200 μL) was added to the mixture followed by its incubation at 37 °C, relative to the blank and control samples. Afterwards, the inhibition activity of the synthesized hybrids was assessed at 475 nm, followed by the measurement of absorbance at this wavelength to determine the rise in dopachrome level. The tyrosinase inhibitory potential of the synthesized conjugates was represented in the form of percentage inhibition and corresponding half-maximal inhibitory concentration values, which were obtained by the extrapolation of the graph. The inferred inhibition activities were compared with that of the standard inhibitors, *i.e.*, kojic and ascorbic acids.

The percentage (%) inhibition of all synthesized conjugates was inferred by the following formula:

$$\text{Percentage inhibition} = (\text{absorbance of blank} - \text{absorbance of sample}/\text{absorbance of control blank}) \times 100$$

Molecular docking analysis

The most potent hybrids **16h** and **16f** were subjected to molecular docking analysis against fungal tyrosinase and human tyrosinase protein. For fungal tyrosinase, the crystalline structure of the protein (6JU7) was attained from the protein data bank (PDB), and was employed as a receptor in the induced fit docking.[71] For the docking analysis against human tyrosinase, homology modelling was carried out by using the Swiss-model online software. The human tyrosinase sequence was copied from the UniProt database (ID: P14679).[72] The crystal structure of human tyrosinase related protein 1 (PDB ID: 5M8T) was selected as the template model on the basis of its identity score (45.81%) with human tyrosinase. The homology modeled structure of the protein was downloaded from the same online software. All of the docking analysis were carried out by utilizing AutoDockTools 1.5.7.[73] The search grid was referred as center_*x*: 15.489, center_*y*:−17.756 and center_*z*: −36.631 for fungal tyrosinase and as center_*x*: 125.361, center_*y*: 287.712 and center_*z*: 211.834 for human tyrosinase with dimensions size_*x*: 40, size_*y*: 40 and size_*z*: 40 for both proteins. The poses with lowest binding scores (obtained by Vina docking score) were chosen and the corresponding ligand–protein interactions were illustrated *via* BIOVIA Discovery Studio 2024.

Molecular dynamics simulation

The protein–ligand complexes were prepared by employing Maestro (Academic version) of Schrödinger LLC to correct the structural defects. The Desmond module was utilized for performing MD simulation analysis to determine the dynamic behavior and structural flexibility of the complexes. The TIP3P[74] solvent model and orthorhombic cubic box features were introduced by using the Desmond[75] system builder. The introduction of counterions, *i.e.*, Na^+ and Cl^-, was done along with the addition of 0.15 M NaCl to impart neutrality and simulate isotonic conditions.[76] The energy of the system was minimized by employing the OPLS2005 force field.[77] An MD simulation was run at 200 ns at 300 K temperature and pressure of 1 atm, generating 1000 trajectories. MD trajectories were analyzed by employing the Simulation Interaction Diagram (SID) to calculate the RMSF, RMSD and protein–ligand contacts. The MMPBSA analysis was also performed by utilizing MD trajectories to determine the binding free energies at different frames of the ligand–protein complexes based on polar solvation, van der Waals, SASA, and electrostatic energies.

ADMET analysis

Both significantly potent synthesized 7-methoxy-benzofuran based hybrids **16h** & **16f** along with standard inhibitors were made to undergo *in silico* ADMET evaluation by using LabADMET 3.0 online software.[78] The SMILES of novel hybrids were generated *via* ChemDraw and the obtained SMILES were run in LabADMET 3.0 to obtain the resulting values of the physiochemical, medicinal, absorption, distribution, metabolism, excretion and toxicity properties.

Conflicts of interest

The authors declare no conflict of interest.

Data availability

The data supporting this article have been included as part of the SI. See DOI: https://doi.org/10.1039/d5ra05084g

Acknowledgements

The authors express their gratitude to Government College University Faisalabad, Pakistan, for providing facilities to carry out this research work. The authors acknowledge and appreciate the Ongoing Research Funding Program (ORF-2025-740), King Saud University, Riyadh, Saudi Arabia.

References

1 E. I. Solomon, U. M. Sundaram and T. E. Machonkin, Multicopper oxidases and oxygenases, *Chem. Rev.*, 1996, **96**, 2563–2606.
2 K. Tief, M. Hahne, A. Schmidt and F. Beermann, Tyrosinase, the key enzyme in melanin synthesis, is expressed in murine brain, *Eur. J. Biochem.*, 1996, **241**, 12–16.
3 C. Belle, in *Encyclopedia of Metalloproteins*, ed. R. H. Kretsinger, V. N. Uversky and E. A. Permyakov, Springer, New York, 2013, pp. 574–579.
4 I. Choi, Y. Park, I. Y. Ryu, H. J. Jung, S. Ullah, H. Choi, C. Park, D. Kang, S. Lee, P. Chun, H. Y. Chung and H. R. Moon, *In silico* and *in vitro* insights into tyrosinase inhibitors with a 2-thioxooxazoline-4-one template, *Comput. Struct. Biotechnol. J.*, 2021, **19**, 37–50.

Open Access Article. Published on 22 September 2025. Downloaded on 1/19/2026 9:13:00 PM. This article is licensed under a Creative Commons Attribution-NonCommercial 3.0 Unported Licence.

5 A. Afshin, M. B. Reitsma and C. J. Murry, Health Effects of Overweight and Obesity in 195 Countries over25 Years, *N. Engl. J. Med.*, 2017, **377**, 13–27.
6 K. Eun Lee, S. Bharadwaj, U. Yadava and S. Gu Kang, Evaluation of caffeine as inhibitor against collagenase, elastase and tyrosinase using *in silico* and *in vitro* approach, *J. Enzyme Inhib. Med. Chem.*, 2019, **34**, 927–936.
7 P. A. Riley and Melanin, *Int. J. Biochem. Cell Biol.*, 1997, **29**, 1235–1239.
8 G.-E. Costin and V. J. Hearing, Human skin pigmentation: melanocytes modulate skin color in response to stress, *FASEB J.*, 2007, **21**, 976–994.
9 A. Slominski, D. J. Tobin, S. Shibahara and J. Wortsman, Melanin pigmentation in mammalian skin and its hormonal regulation, *Physiol. Rev.*, 2004, **84**, 1155–1228.
10 A. Slominski, J. Wortsman, P. M. Plonka, K. U. Schallreuter, R. Paus and D. J. Tobin, Hair follicle pigmentation, *J. Invest. Dermatol.*, 2005, **124**, 13–21.
11 L. Feng, N. Shi, S. Cai, X. Qiao, P. Chu, H. Wang, F. Long, H. Yang, Y. Yang, Y. Wang and H. Yu, De novo molecular design of a novel octapeptide that inhibits *in vivo* melanogenesis and has great transdermal ability, *J. Med. Chem.*, 2018, **61**, 6846–6857.
12 W.-C. Chen, T.-S. Tseng, N.-W. Hsiao, Y.-L. Lin, Z.-H. Wen, C.-C. Tsai, Y.-C. Lee, h.-h. Lin and K.-C. Tsai, Discovery of highly potent tyrosinase inhibitor, T1, with significant *anti*-melanogenesis ability by zebrafish *in vivo* assay and computational molecular modeling, *Sci. Rep.*, 2015, **5**, 7995.
13 J. Y. Lee, H. J. Choi, T. W. Chung, C. H. Kim, H. S. Jeong and K. T. Ha, Caffeic acid phenethyl ester inhibits alpha-melanocyte stimulating hormone-induced melanin synthesis through suppressing transactivation activity of microphthalmia-associated transcription factor, *J. Nat. Prod.*, 2013, **76**, 1399–1405.
14 M. Y. Noh, S. Muthukrishnan, K. J. Kramer and Y. Arakane, Cuticle formation and pigmentation in beetles, *Curr. Opin. Insect Sci.*, 2016, **17**, 1–9.
15 R. Jiang, X.-H. Xu, K. Wang, X.-Z. Yang, Y.-F. Bi, Y. Yan, J.-Z. Liu, N.-N. Chen, Z.-Z. Wang, X.-L. Guo, D.-Q. Zhao and L.-W. Sun, Ethyl acetate extract from Panax ginseng CA Meyer and its main constituents inhibit α-melanocyte-stimulating hormone-induced melanogenesis by suppressing oxidative stress in B16 mouse melanoma cells, *J. Ethnopharmacol.*, 2017, **208**, 149–156.
16 Y. L. Shi, I. F. Benzie and J. A. Buswell, Role of tyrosinase in the genoprotective effect of the edible mushroom. Agaricus Bisporus, *Life Sci.*, 2002, **70**, 1595–1608.
17 T. Kobayashi, W. D. Vieira, B. Potterf, C. Sakai, G. Imokawa and V. J. Hearing, Modulation of melanogenic protein expression during the switch from eu-to pheomelanogenesis, *J. Cell Sci.*, 1995, **108**, 2301–2309.
18 T. Pillaiyar, M. Manickam and V. Namasivayam, Skin whitening agents: medicinal chemistry perspective of tyrosinase inhibitors, *J. Enzyme Inhib. Med. Chem.*, 2017, **32**, 403–425.
19 E. L. Cavalieri, K. M. Li, N. Balu, M. Saeed, P. Devanesan, S. Higginbotham, J. Zhao, M. L. Gross and E. G. Rogan, Catechol ortho-quinones: the electrophilic compounds that form depurinating DNA adducts and could initiate cancer and other diseases, *Carcinogenesis*, 2002, **23**, 1071–1077.
20 A. Vontzalidou, G. Zoidis, E. Chaita, M. Makropoulou, N. Aligiannis, G. Lambrinidis, E. Mikros and A. L. Skaltsounis, Design, synthesis and molecular simulation studies of dihydrostilbene derivatives as potent tyrosinase inhibitors, *Bioorg. Med. Chem. Lett.*, 2012, **22**, 5523–5526.
21 T. Hasegawa, Tyrosinase-expressing neuronal cell line as *in vitro* model of Parkinson's disease, *Int. J. Mol. Sci.*, 2010, **11**, 1082–1089.
22 I. Tessari, M. Bisaglia, F. Valle, B. Samorì, E. Bergantino, S. Mammi and L. Bubacco, The reaction of α-synuclein with tyrosinase: possible implications for Parkinson disease, *J. Biol.Chem.*, 2008, **283**, 16808–16817.
23 E. Greggio, E. Bergantino, D. Carter, R. Ahmad, G. E. Costin, V. J. Hearing, J. Clarimon, A. Singleton, J. Eerola, O. Hellström and P. J. Tienari, Tyrosinase exacerbates dopamine toxicity but is not genetically associated with Parkinson's disease, *J. Neurochem.*, 2005, **93**, 246–256.
24 S. Nithitanakool, P. Pithayanukul, R. Bavovada and P. Saparpakorn, Molecular docking studies and *anti*-tyrosinase activity of Thai mango seed kernel extract, *Molecules*, 2009, **14**, 257–265.
25 N. Brotzman, Y. Xu, A. Graybill, A. Cocolas, A. Ressler, N. P. Seeram, H. Ma and G. E. Henry, Synthesis and tyrosinase inhibitory activities of 4-oxobutanoate derivatives of carvacrol and thymol, *Bioorg. Med. Chem. Lett.*, 2019, **29**, 56–58.
26 B. Lee, K. M. Moon, B.-S. Lee, J.-H. Yang, K.-I. Park, W.-K. Cho and J.-Y. Ma, Swertiajaponin inhibits skin pigmentation by dual mechanisms to suppress tyrosinase, *Oncotarget*, 2017, **8**, 95530–95541.
27 L.-J. Juang, X.-Y. Gao, S.-T. Mai, C.-H. Lee, M.-C. Lee and C.-L. Yao, Safety assessment, biological effects, and mechanisms of Myrica rubra fruit extract for antimelanogenesis, *anti*-oxidation, and free radical scavenging abilities on melanoma cells, *J. Cosmet. Dermatol.*, 2019, **18**, 322–332.
28 S. B. Kim, Y. H. Jo, Q. Liu, J. H. Ahn, I. P. Hong, S. M. Han, B. Y. Hwang and M. K. Lee, Optimization of extraction condition of bee pollen using response surface methodology: correlation between *anti*-melanogenesis, antioxidant activity, and phenolic content, *Molecules*, 2015, **20**, 19764–19774.
29 H. X. Li, J. U. Park, X. D. Su, K. T. Kim, J. S. Kang, Y. R. Kim, Y. H. Kim and S. Y. Yang, Identification of *anti*-melanogenesis constituents from *Morus alba* L. leaves, *Molecules*, 2018, **23**, 2559.
30 W. Yi, R. Cao, W. Peng, H. Wen, Q. Yan, B. Zhou, L. Ma and H. Song, Synthesis and biological evaluation of novel 4-hydroxybenzaldehyde derivatives as tyrosinase inhibitors, *Eur. J. Med. Chem.*, 2010, **45**, 639–646.
31 M. Friedman, Food browning and its prevention: an overview, *J. Agric. Food Chem.*, 1996, **44**, 631–653.

© 2025 The Author(s). Published by the Royal Society of Chemistry

Open Access Article. Published on 22 September 2025. Downloaded on 1/19/2026 9:13:00 PM. This article is licensed under a Creative Commons Attribution-NonCommercial 3.0 Unported Licence.

32 A. M. Mayer, Polyphenol oxidases in plants-recent progress, *Phytochemistry*, 1986, **26**, 11–12.
33 M. N. Masum, K. Yamauchi and T. Mitsunaga, Tyrosinase inhibitors from natural and synthetic sources as skin-lightening agents, *Rev. Agric. Sci.*, 2019, **7**, 41–58.
34 Y. Matoba, T. Kumagai, A. Yamamoto, H. Yoshitsu and M. Sugiyama, Crystallographic evidence that the dinuclear copper center of tyrosinase is flexible during catalysis, *J. Biol. Chem.*, 2006, **281**, 8981–8990.
35 N. J. Bentley, T. Eisen and C. R. Goding, Melanocyte-specific expression of the human tyrosinase promoter: activation by the microphthalmia gene product and role of the initiator, *Mol. Cell. Biol.*, 1994, **14**, 7996–8006.
36 W. Zhu and J. Gao, The use of botanical extracts as topical skin-lightening agents for the improvement of skin pigmentation disorders, *J. Invest. Dermatol. Symp. Proc.*, 2008, **13**, 20–24.
37 S. L. Cheng, L. R. Huang, J. N. Sheu, S. T. Chen, S. Sinchaikul and G. J. Tsay, Toxicogenomics of kojic acid on gene expression profiling of a375 human malignant melanoma cells, *Biol. Pharm. Bull.*, 2006, **29**, 655–669.
38 G. A. Burdock, M. G. Soni and I. G. Carabin, Evaluation of health aspects of kojic acid in food, *Regul. Toxicol. Pharmacol.*, 2001, **33**, 80–101.
39 E. Kabir, M. Uzzaman and M. A, review on biological and medicinal impact of heterocyclic compounds, *Results Chem.*, 2022, **4**, 100606.
40 R. Saeed, M. Usman, N. Rasool, M. Ahmad, Z. A. Khan, Z. H. Farooqi, M. Siddiq and A. F. Zahoor, Partitioning of thiophene derivatives between solvent and micellar media of cationic surfactant, cetyl trimethyl ammonium bromide, *J. Mol. Liq.*, 2017, **240**, 389–394.
41 A. Mushtaq, A. F. Zahoor, M. Bilal, S. M. Hussain, M. Irfan, R. Akhtar, A. Irfan, K. Kotowica-Mojzych and M. Mojzych, Sharpless asymmetric dihydroxylation: an impressive gadget for the synthesis of natural products: a review, *Molecules*, 2023, **28**, 2722.
42 R. Akhtar, A. F. Zahoor, M. Irfan, T. H. Bokhari and A. ul Haq, Recent green synthetic approaches toward Ullmann reaction: a review, *Chem. Pap.*, 2022, **76**, 7275–7293.
43 K. Chand, A. Hiremathad, M. Singh, M. A. Santos and R. S. Keri, A review on antioxidant potential of bioactive heterocycle benzofuran: natural and synthetic derivatives, *Pharmacol. Rep.*, 2017, **69**, 281–295.
44 K. M. Dawood, Benzofuran derivatives: a patent review, *Expert Opin. Ther. Pat.*, 2013, **23**, 1133–1156.
45 A. Radadiya and A. Shah, Bioactive benzofuran derivatives: an insight on lead developments, radioligands and advances of the last decade, *Eur. J. Med. Chem.*, 2015, **97**, 356–376.
46 M. Napiórkowska, M. Cieślak, J. Kaźmierczak-Barańska, K. Królewska-Golińska and B. Nawrot, Synthesis of new derivatives of benzofuran as potential anticancer agents, *Molecules*, 2019, **24**, 1529.
47 R. Naik, D. S. Harmalkar, X. Xu, K. Jang and K. Lee, Bioactive benzofuran derivatives: Moracins A–Z in medicinal chemistry, *Eur. J. Med. Chem.*, 2015, **90**, 379–393.
48 S. A. Galal, A. S. Abd El-All, M. M. Abdallah and H. I. El-Diwani, Synthesis of potent antitumor and antiviral benzofuran derivatives, *Bioorg. Med. Chem. Lett.*, 2009, **19**, 2420–2428.
49 X. Jiang, W. Liu, W. Zhang, F. Jiang, Z. Gao, H. Zhuang and L. Fu, Synthesis and antimicrobial evaluation of new benzofuran derivatives, *Eur. J. Med. Chem.*, 2011, **46**, 3526–3530.
50 D. Dwarakanath and S. L. Gaonkar, Advances in synthetic strategies and medicinal importance of benzofurans: a review, *Asian J. Org. Chem.*, 2022, **11**, e202200282.
51 A. Irfan, S. Faisal, A. F. Zahoor, R. Noreen, S. A. Al-Hussain, B. Tuzun, R. Javaid, A. A. Elhenawy, M. E. A. Zaki, S. Ahmad and M. H. Abdellattif, *In Silico* Development of Novel Benzofuran-1,3,4-Oxadiazoles as Lead Inhibitors of M. tuberculosis Polyketide Synthase 13, *Pharmaceuticals*, 2023, **16**, 829.
52 Z. Xu, S. Zhao, Z. Lv, L. Feng, Y. Wang, F. Zhang, L. Bai and J. Deng, Benzofuran derivatives and their *anti*-tubercular, *anti*-bacterial activities, *Eur. J. Med. Chem.*, 2019, **162**, 266–276.
53 J. Farhat, L. Alzyoud, M. Alwahsh and B. Al-Omari, Structure–activity relationship of benzofuran derivatives with potential anticancer activity, *Cancers*, 2022, **14**, 2196.
54 M. Toeller, Diabetes Research Institute, Clinical Department, Heinrich-Heine-University, Diisseldorf, Germany, a-Glucosidase inhibitors in diabetes: efficacy in NIDDM subjects, *Eur. J. Clin. Invest.*, 1994, **24**, 31–35.
55 Y. H. Miao, Y. H. Hu, J. Yang, T. Liu, J. Sun and X. J. Wang, Natural source, bioactivity and synthesis of benzofuran derivatives, *RSC Adv.*, 2019, **9**, 27510–27540.
56 A. A. Abbas and K. M. Dawood, Anticancer therapeutic potential of benzofuran scaffolds, *RSC Adv.*, 2023, **13**, 11096–11120.
57 A. Irfan, A. F. Zahoor, A. Rasul, S. A. Al-Hussain, S. Faisal, S. Ahmad, R. Noor, M. T. Muhammed and M. E. A. Zaki, BTEAC Catalyzed Ultrasonic-Assisted Synthesis of Bromobenzofuran-Oxadiazoles: Unravelling Anti-HepG-2 Cancer Therapeutic Potential through *In Vitro* and *In Silico* Studies, *Int. J. Mol. Sci.*, 2023, **24**, 3008.
58 A. Irfan, S. Faiz, A. Rasul, R. Zafar, A. F. Zahoor, K. Kotwica-Mojzych and M. Mojzych, Exploring the Synergistic Anticancer Potential of Benzofuran–Oxadiazoles and Triazoles: Improved Ultrasound- and Microwave-Assisted Synthesis, Molecular Docking, Hemolytic, Thrombolytic and Anticancer Evaluation of Furan-Based Molecules, *Molecules*, 2022, **27**, 1023B.
59 P. Patel, R. Shakya, V. Asati, B. D. Kurmi, S. K. Verma, G. D. Gupta and H. Rajak, Furan and benzofuran derivatives as privileged scaffolds as anticancer agents: SAR and docking studies (2010 to till date), *J. Mol. Struct.*, 2023, **1299**, 137098.
60 S. N. Aslam, P. C. Stevenson, S. J. Phythian, N. C. Veitch and D. R. Hall, Synthesis of cicerfuran, an antifungal benzofuran, and some related analogues, *Tetrahedron*, 2006, **62**, 4214–4226.

Open Access Article. Published on 22 September 2025. Downloaded on 1/19/2026 9:13:00 PM. This article is licensed under a Creative Commons Attribution-NonCommercial 3.0 Unported Licence.

61 A. Hiremathad, M. R. Patil, K. R. Chethana, K. Chand, M. A. Santos and R. S. Keri, Benzofuran: an emerging scaffold for antimicrobial agents, *RSC Adv.*, 2015, **5**, 96809–96828.

62 A. Irfan, S. Faisal, S. Ahmad, M. J. Saif, A. F. Zahoor, S. G. Khan, J. Javid, S. A. Al-Hussain, M. T. Muhammed and M. E. A. Zaki, An Exploration of the Inhibitory Mechanism of Rationally Screened Benzofuran-1,3,4-Oxadiazoles and-1,2,4-Triazoles as Inhibitors of NS5B RdRp Hepatitis C Virus through Pharmacoinformatic Approaches, *Biomedicines*, 2023, **11**, 3085.

63 L. Arce-Ramos, J. C. Castillo and D. Becerra, Synthesis and Biological Studies of Benzo [b] furan Derivatives: A Review from 2011 to 2022, *Pharmaceuticals*, 2023, **16**, 1265.

64 B. Carlsson, B. N. Singh, M. Temciuc, S. Nilsson, Y. L. Li, C. Mellin and J. Malm, Synthesis and preliminary characterization of a novel antiarrhythmic compound (KB130015) with an improved toxicity profile compared with amiodarone, *J. Med. Chem.*, 2002, **45**, 623–630.

65 D. W. Holt, G. T. Tucker, P. R. Jackson and G. C. Storey, Amiodarone pharmacokinetics, *Am. Heart J.*, 1983, **106**, 840–847.

66 A. Irfan, A. F. Zahoor, S. Kamal, M. Hassan and A. Kloczkowski, Ultrasonic-assisted synthesis of benzofuran appended oxadiazole molecules as tyrosinase inhibitors: mechanistic approach through enzyme inhibition, molecular docking, chemoinformatics, ADMET and drug-likeness studies, *Int. J. Mol. Sci.*, 2022, **23**, 10979.

67 A. Irfan, S. Faisal, S. Ahmad, S. A. Al-Hussain, S. Javed, A. F. Zahoor, B. Parveen, M. E. Zaki and M. E. Structure-Based, Virtual Screening of Furan-1, 3, 4-Oxadiazole Tethered N-phenylacetamide Derivatives as Novel Class of hTYR and hTYRP1 Inhibitors, *Pharmaceuticals*, 2023, **16**, 344.

68 R. Kausar, A. F. Zahoor, H. Tabassum, S. Kamal and M. Ahmad Bhat, Synergistic biomedical potential and molecular docking analyses of coumarin–triazole hybrids as tyrosinase inhibitors: design, synthesis, *in vitro* profiling, and *in silico* studies, *Pharmaceuticals*, 2024, **17**, 532.

69 M. Hassan, Z. Ashraf, Q. Abbas, H. Raza and S. Y. Seo, Exploration of novel human tyrosinase inhibitors by molecular modeling, docking and simulation studies, *Interdiscip. Sci. Comput. Life Sci.*, 2018, **10**, 68–80.

70 J. H. Kim, J.-Y. Yoon, S. Y. Yang, S.-K. Choi, S. J. Kwon, I. S. Cho, M. H. Jeong, Y. Ho Kim and G. S. Choi, Tyrosinase inhibitory components from Aloevera and their antiviral activity, *J. Enzym. Inhib. Med. Chem.*, 2017, **32**, 78–83.

71 N. Fujieda, K. Umakoshi, Y. Ochi, Y. Nishikawa, S. Yanagisawa, M. Kubo, G. Kurisu and S. Itoh, Copper–oxygen dynamics in the tyrosinase mechanism, *Angew. Chem.*, 2020, **132**, 13487–13492.

72 I. Choi, Y. Park, I. Y. Ryu, H. J. Jung, S. Ullah, H. Choi, C. Park, D. Kang, S. Lee, P. Chun, H. Y. Chung and H. R. Moon, *In silico* and *in vitro* insights into tyrosinase inhibitors with a 2-thioxooxazoline-4-one template, *Comput. Struct. Biotec.*, 2021, **19**, 37–50.

73 G. Wang, Z. Peng, J. Wang, X. Li and X. J. Li, Synthesis, *in vitro* evaluation and molecular docking studies of novel triazine-triazole derivatives as potential α-glucosidase inhibitors, *Eur. J. Med. Chem.*, 2017, **125**, 423–429.

74 Y. Moukhliss, Y. Koubi, M. Alaqarbeh, N. Alsakhen, S. Hamzeh, H. Maghat, A. Sbai, M. Bouacchrine and T. Lakhlifi, A study of drug candidates derived from pleconaril for inhibiting coxsackievirus B3 (Cvb3) by ADMET, molecular docking, molecular dynamics and retrosynthesis, *New J. Chem.*, 2022, **46**, 10154–10161.

75 Y. Ali, A. A. Khan, A. M. Alanazi, S. A. Abdikakharovich, J. A. Shah, Z. G. Ren and S. Khatatak, Identification of the myxobacterial secondary metabolites Aurachin A and Soraphinol A as promising inhibitors of thymidylate kinase of the Monkeypox virus, *Mol. Divers.*, 2024, **28**, 3349–3362.

76 B. Jójárt, R. Kiss, B. Viskolcz, I. Kolossváry and G. M. Keserű, Molecular dynamics simulation at high sodium chloride concentration: toward the inactive conformation of the human adenosine A2A receptor, *J. Phys. Chem. Lett.*, 2010, **1**, 1008–1013.

77 Y. Hua, X. Tan, J. Zhang, N. Xu, R. Chen, S. Zhou, S. Liu, K. Li, W. Chen, Q. Luo and Y. Li, Deciphering the pharmacological mechanism of Radix astragali for allergic rhinitis through network pharmacology and experimental validation, *Sci. Rep.*, 2024, **14**, 29873.

78 L. Fu, S. Shi, J. Yi, N. Wang, Y. He, Z. Wu, J. Peng, Y. Deng, W. Wang, C. Wu, A. Lyu, X. Zeng, W. Zhao, T. Hou and D. Cao, ADMETlab 3.0: an updated comprehensive online ADMET prediction platform enhanced with broader coverage, improved performance, API functionality and decision support, *Nucleic Acids Res.*, 2024, **52**, W422–W431.

© 2025 The Author(s). Published by the Royal Society of Chemistry